Commun Nonlinear Sci Numer Simulat 157 (2026) 109666

Contents lists available at ScienceDirect

Communications in Nonlinear Science and Numerical Simulation

journal homepage: www.elsevier.com/locate/cnsns

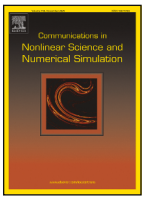

Research paper

# Spatial sampling-based passivity and synchronization of multiweighted coupled reaction-diffusion neural networks

Haodong Cui [a], Haoyun Tang [a], Mingyu Ma [a], Cheng Hu [a,b,*], Tingting Shi [a]

[a] College of Mathematics and System Science, Xinjiang University, 830017, Urumqi, China
[b] Xinjiang Key Laboratory of Applied Mathematics (XJDX1401), 830017, Urumqi, China

ARTICLE INFO

*Keywords:*
Coupled neural networks
Spatial sampling control
Passivity and synchronization
Multiweighted coupling
Adaptive control

ABSTRACT

A type of multiweighted coupled reaction-diffusion neural networks with general delays is formulated in this study, and the passivity and synchronization are addressed via spatial sampling control. Firstly, an innovative spatial sampling controller is developed, which is distributed at the midpoint of each spatial sampling interval and improves traditional full-domain control schemes. Additionally, by utilizing variable rearrangement technique and constructing some Lyapunov-Krasovskii functionals, several passivity and synchronization criteria presented by LMIs are derived. Moreover, to further reduce the control cost, an adaptive spatial sampling control strategy is proposed and the adaptive synchronization is rigorously analyzed. Note that only the weighted union topology of all coupling layers is constrained to be connected, which relaxes the previous requirement on the strong connectivity of each coupling topology. The obtained results are confirmed by an illustrative example and are applied to image encryption and decryption.

## 1. Introduction

Over recent decades, coupled neural networks (CNNs) have attracted widespread attention due to their extensive applications in addressing complex practical problems, such as pattern recognition, associative memory and quadratic optimization [1–3]. However, most of these models are described by a single coupling, irrespective of the complexity of the relationships among real individuals. Although the use of a single coupling model offers the advantages of simplicity and ease of analysis, this simplification might lead to an incomplete understanding of the system's complexity. For instance, in social networks, individuals communicate via multiple channels, including media platforms, emails and phone calls [4]. Similarly, the complexity of controlling COVID-19 has been intensified by its multiple transmission routes like person-to-person, fomite-to-person and environmental-to-person transmission [5]. To capture the richness of these interactions, network models incorporate multi-weighted couplings, which have important applications in biological network modeling, multi-modal data processing and economic systems [6–8].

Passivity, as a fundamental property of physical systems, characterizes the energy dissipation behavior via the system's intrinsic energy storage dynamics and its external input-output relationships. Specifically, a passive system is a physical system with inherent dissipative components, in which the accumulated stored energy for any arbitrary time durations is less than or equal to the energy supplied through external inputs [9]. Typical examples include resistors, capacitors, and inductors in electrical circuits [10]. This property implies that the system cannot generate energy by itself but can only dissipate energy supplied by external sources.

* Corresponding author.
*E-mail addresses:* haotungcui@163.com (H. Cui), haoyuntang224@163.com (H. Tang), mingyuma0829@163.com (M. Ma), hucheng@xju.edu.cn (C. Hu), 107556521092@stu.xju.edu.cn (T. Shi).

https://doi.org/10.1016/j.cnsns.2026.109666
Received 5 April 2025; Received in revised form 5 July 2025; Accepted 6 January 2026
Available online 8 January 2026

Consequently, passivity provides a powerful criterion for guaranteeing the intrinsic stability of systems [11]. Given its widespread utility in diverse domains such as mechanical systems and power networks, the passivity of CNNs has garnered growing interest, and a large number of excellent achievements have emerged [12–15]. Wang et al. [12] conducted a rigorous passivity analysis for CNNs with multi-weighted couplings, and passivity conditions were derived for systems with mismatched input-output dimensions. By employing the variable rearrange order technique, Lin and Liu addressed the passivity and control of multi-coupled dynamical networks [14].

Note that, the above considerable efforts are mainly devoted to CNNs modeled by ordinary differential systems, where the dynamic evolution merely depends on the time. However, these models neglect the spatial evolution of neurons and are unable to accurately explain the flow of neuronal information as well as the inter-layer information exchange among neurons in biological systems [16,17]. To accurately depict the spatiotemporal dynamics and interactions of neurons, the reaction-diffusion term is introduced into CNNs. Recently, passivity analysis and passivity-based control of reaction-diffusion neural networks (RDNNs) have been increasingly reported [18–21]. In [18], by establishing the definition of fixed-time passivity, some fixed-time passification conditions for memristive reaction-diffusion neural networks were obtained via nonlinear full-domain control. In practice, time delays are inevitable due to the limited bandwidth and the constrained transmission speed during information transmission [20]. In view of this, based on Lyapunov Krasovskii functionals method, Huang et al. [21] explored the passivity of multi-weighted RDNNs with time-varying delays via full-domain event-triggered controller. In [22], the input and output passivity of RDNNs with multi-proportional delays was addressed by constructing a Lyapunov Krasovskii functional. More importantly, Wang et al. [23,24] further extended the theory of passivity to investigate the synchronization of CNNs. Specifically, the synchronization problem of CNNs was reformulated as the stability analysis of an error system. When the external input is removed, the original CNNs achieves synchronization if the error system exhibits output-strict passivity. Since the concept of output-strict passivity was introduced, the problem of passivity-based control for synchronization of RDNNs has received considerable attention [25–27]. In [25], an adaptive pinning controller was designed to realize both passivity and synchronization in fractional spatiotemporal networks. Considering time delay and parameter uncertainties, Lin et al. studied passivity and synchronization of multiple-weighted RDNNs by designing an event-triggered controller in [26]. Note that, the aforementioned studies are exclusively concentrated on RDNNs characterized by the single time delay. However, in practical engineering and technical fields, a system may be simultaneously affected by multiple time-delay factors, such as constant delay, time-varying delay, distributed delay, and proportional delay [28–31]. Unfortunately, integrating these time delays into a unified system model and analyzing passivity and synchronization for RDNNs with multiple delays remain a challenging task.

It is important to highlight that the aforementioned passivity-based controllers require actuators to be distributed throughout the entire interior space domain. This requirement ensures that control actions can be applied continuously across the spatial dimension, which often involves high costs and technical challenges in the engineering implementation. For example, in large-scale systems such as the control of concentration and temperature in chemical reactors or the installation of traffic signal lights and surveillance equipment in the transportation network, it is difficult to achieve full-domain control due to technical or economic limitations. In contrast, spatial sampled-data control can achieve the desired control objective by distributing actuators at specific spatial points rather than across the entire domain [32]. Owing to its significant advantages, including the ease of installation, cost-effectiveness and high efficiency, this approach has garnered considerable attention in both academic and practical fields [33–39]. Lu et al. [34] developed a kind of spacial sampled-data controller for $H_\infty$ output synchronization of RDNNs with discrete and distributed delays, in which the actuators are placed at the midpoint of each sampling interval. In [35] and [36], a spatial sampled-data controller was presented to realize synchronization of RDNNs with and without mixed delays, and several consitions formed by linear matrix inequalities (LMI) were derived by constructing a Lyapunov Krasovskii functional. Based on spatially averaged measurements and the method of Lyapunov Krasovskii functionals, the dissipativity behavior of delayed RDNNs was analysed via adaptive event-triggered sampled-data control in [37]. Unlike the technique of Lyapunov Krasovskii functionals, the cluster synchronization criteria for delayed genetic regulatory networks were derived based on Halanay's inequality under an intermittent space-dividing controller in [38]. Compared with the abundant achievements in the sampled-data synchronization of RDNNs, the passivity analysis of delayed RDNNs under spatial sampling control has not been systematically and deeply explored. Given the diverse coupling structures and complex dynamic behaviors of delayed RDNNs, how to design efficient passivity-based sampling control strategies under spatial point measurements, and how to establish the intrinsic relationship between passivity and synchronization, are key scientific issues that need to be urgently addressed.

Inspired by the above discussion, the passivity and synchronization of delayed RDNNs with multi-weighted coupling are investigated in this article. Several sufficient conditions for passivity and synchronization are established by designing spatial sampling controllers. The main highlights of this article are summarized as follows.

(1) To capture the influence of different delays on the system and the richness of neural network interactions, a class of RDNNs with multi-weighted coupling is formulated which integrates discrete time delays [23,37,38], distributed delays [34,35,40], and proportional delays [22,28].

(2) To realize passivity and synchronization, a spatial sampling controller distributed at the midpoint of each sampling interval is designed, which is more economical and convenient than the full-domain control presented in [25–27]. To further reduce the control gains determined by the LMI condition, an adaptive spatial sampling control strategy is developed to dynamically update the control gain and finally achieve asymptotical synchronization.

(3) By constructing some Lyapunov Krasovskii functionals, several passivity and passivity-based synchronization criteria are derived for the RDNNs with mismatched input and output dimensions. In theoretical analysis, the requirement for strong connectivity of each coupling layer of communication topology, as considered in [6–8,34], is relaxed to the connectivity about the union graph through the variable rearrangement technique.

**Table 1**
Notations and Definitions.

| Notations | Definitions |
|---|---|
| $\mathbb{N}^+, \overline{1,\mathcal{N}}, \mathcal{R}_{\geq 0}$ | $\mathbb{N}^+ = \{1,2,\dots\}, \overline{1,\mathcal{N}} = \{1,2,\dots,\mathcal{N}\}, \mathcal{R}_{\geq 0} = [0,+\infty)$ |
| $\mathcal{R}^n, \mathcal{R}^{n\times m}$ | The space of all $n$-dimensional real vectors/$n\times m$ real matrices |
| $\mathcal{M} > 0 (< 0)$ | The symmetric matrix $\mathcal{M}$ is positive definite (negative definite) |
| $[\mathcal{M}]^s$ | $[\mathcal{M}]^s = \frac{\mathcal{M}^T+\mathcal{M}}{2}$ |
| $\|v\|_2$ | $\|v\|_2 = \sqrt{v^T v}$ with $v \in \mathcal{R}^n$ |
| $\|z(t,\cdot)\|_{[\underline{\alpha},\bar{\alpha}]}$ | $\|z(t,\cdot)\|_{[\underline{\alpha},\bar{\alpha}]} = (\int_{\underline{\alpha}}^{\bar{\alpha}} z^T(t,\varsigma)z(t,\varsigma)\mathrm{d}\varsigma)^{\frac{1}{2}}$ with $\underline{\alpha} < \bar{\alpha}$, $t \in \mathcal{R}_{\geq 0}$, $z(t,\varsigma) \in \mathcal{R}^n$ |
| $\mathbf{0}_n, \mathbf{1}_n$ | $\mathbf{0}_n = (0,0,\dots,0)^T \in \mathcal{R}^n, \mathbf{1}_n = (1,1,\dots,1)^T \in \mathcal{R}^n$ |
| $\mathbf{I}_n$ | $n$-order identity matrix |

The notations used in this article are provided in Table 1.

## 2. Preparation and problem formation

Consider a kind of multi-weighted coupled reaction-diffusion neural networks with mixed time-varying delay, which is depicted as

$$\begin{aligned}\frac{\partial z_i(t,\varsigma)}{\partial t} =& \mathcal{D}\frac{\partial^2 z_i(t,\varsigma)}{\partial \varsigma^2} - \mathcal{A}z_i(t,\varsigma) + \mathcal{B}_1 f_1\big(z_i(t,\varsigma)\big) + \mathcal{B}_2 f_2\big(z_i(\varrho(t),\varsigma)\big)\\ &+ \mathcal{B}_3\int_{t-\iota(t)}^{t} f_3\big(z_i(\upsilon,\varsigma)\big)\mathrm{d}\upsilon + \sum_{\eta=1}^{\sigma}\sum_{j=1}^{\mathcal{N}} c^\eta g_{ij}^\eta \Gamma^\eta z_j(t,\varsigma)\\ &+ \omega_i(t,\varsigma) + u_i(t,\varsigma), \quad i \in \overline{1,\mathcal{N}},\end{aligned} \tag{1}$$

where $t \in \mathcal{R}_{\geq 0}$, $\varsigma \in (\underline{\alpha},\bar{\alpha})$, $z_i(t,\varsigma) = (z_i^1(t,\varsigma), z_i^2(t,\varsigma),\dots,z_i^n(t,\varsigma))^T \in \mathcal{R}^n$ is the state of the $i$-th neural network, $f_r(z_i(\cdot)) = (f_r^1(z_i^1(\cdot)), f_r^2(z_i^2(\cdot)),\dots,f_r^n(z_i^n(\cdot)))^T \in \mathcal{R}^n$ is the nonlinear activation function ($r = 1,2,3$), $\omega_i(t,\varsigma) \in \mathcal{R}^n$ is the external input, $u_i(t,\varsigma) \in \mathcal{R}^n$ is a spatial sampling controller , $\varrho(t)$ denotes the general time-varying delay, $\iota(t)$ represents the distributed time-varying delay, $\mathcal{D} = \mathrm{diag}\{d_1,d_2,\dots,d_n\} > 0$ is the diffusion coefficient matrix, $\mathcal{A} = \mathrm{diag}\{a_1,a_2,\dots,a_n\}$, $a_k > 0$ denotes the potential decay rate of the $k$-th neuron toward its resting state, $\mathcal{B}_r = (b_{ij}^r)_{n\times n}$ ($r \in \overline{1,3}$) are the synaptic connection weights between neurons, $c^\eta > 0$ and $\Gamma^\eta = \mathrm{diag}\{\gamma_1^\eta,\gamma_2^\eta,\dots,\gamma_n^\eta\} > 0$ are the coupling strength and the inner coupling matrix of the $\eta$-th coupling, respectively. $G^\eta = (g_{ij}^\eta)_{\mathcal{N}\times\mathcal{N}}$ represents the outer coupling matrix of the $\eta$-th coupling, where $g_{ij}^\eta > 0$ ($i \neq j$) if there is communication from node $j$ to node $i$, otherwise, $g_{ij}^\eta = 0$, and $g_{ii}^\eta = -\sum_{j=1,j\neq i}^{\mathcal{N}} g_{ij}^\eta$.

**Assumption 1.** For any nonlinear function $f_r(\cdot) : \mathcal{R}^n \to \mathcal{R}^n$ ($r \in \overline{1,3}$), there exists a positive constant $L_r$ such that

$$\|f_r(z) - f_r(z^*)\|_2 \leq \sqrt{L_r}\|z - z^*\|_2, \quad z, z^* \in \mathcal{R}^n.$$

**Assumption 2.** There exist positive constants $\hat{\varrho}$, $\bar{\varrho}$ and $\bar{\iota}$ such that

$$t \leq \varrho(t) + \bar{\varrho}, \quad 0 < \hat{\varrho} \leq \dot{\varrho}(t), \quad \iota(t) \leq \bar{\iota}.$$

The Dirichlet boundary condition and the initial state of system (1) are given as

$$\begin{cases} z_i(t,\underline{\alpha}) = z_i(t,\bar{\alpha}) = \mathbf{0}_n, & t \in [-\iota,+\infty),\\ z_i(t,\varsigma) = \phi_i(t,\varsigma), & (t,\varsigma) \in [-\iota,0]\times(\underline{\alpha},\bar{\alpha}),\end{cases} \tag{2}$$

where $\iota = \max\{-\varrho(0),\bar{\iota}\}$ with $\varrho(0) \leq 0$, and $\phi_i(t,\varsigma) = (\phi_i^1(t,\varsigma),\phi_i^2(t,\varsigma),\dots,\phi_i^n(t,\varsigma))^T \in \mathcal{R}^n$ is a continuous function.

**Remark 1.** Assumption 1 is a common Lipschitz condition, which is used to guarantee the existence of the solution of the system (1). The function $\varrho(t)$ in Assumption 2 represents a generalized form of time-delay. Specifically, if $\varrho(t) = t - h(t)$ with $0 \leq h(t) \leq h$, then $\varrho(t)$ reduces to a discrete time-delay as discussed in [23,37,38]. If $\varrho(t) = pt$ with $0 < p < 1$, it simplifies to a proportional delay, which has been explored in [28].

From $z_i(t,\varsigma) = (z_i^1(t,\varsigma), z_i^2(t,\varsigma),\dots,z_i^n(t,\varsigma))^T$, system (1) is represented in the following scalar form

$$\begin{aligned}\frac{\partial z_i^k(t,\varsigma)}{\partial t} =& d_k\frac{\partial^2 z_i^k(t,\varsigma)}{\partial \varsigma^2} - a_k z_i^k(t,\varsigma) + \sum_{s=1}^{n} b_{ks}^1 f_1^s\big(z_i^s(t,\varsigma)\big)\\ &+ \sum_{s=1}^{n} b_{ks}^2 f_2^s\big(z_i^s(\varrho(t),\varsigma)\big) + \sum_{s=1}^{n} b_{ks}^3\int_{t-\iota(t)}^{t} f_3^s\big(z_i^s(\upsilon,\varsigma)\big)\mathrm{d}\upsilon\\ &+ \sum_{\eta=1}^{\sigma}\sum_{j=1}^{\mathcal{N}} c^\eta g_{ij}^\eta \gamma_k^\eta z_j^k(t,\varsigma) + \omega_i^k(t,\varsigma) + u_i^k(t,\varsigma).\end{aligned} \tag{3}$$

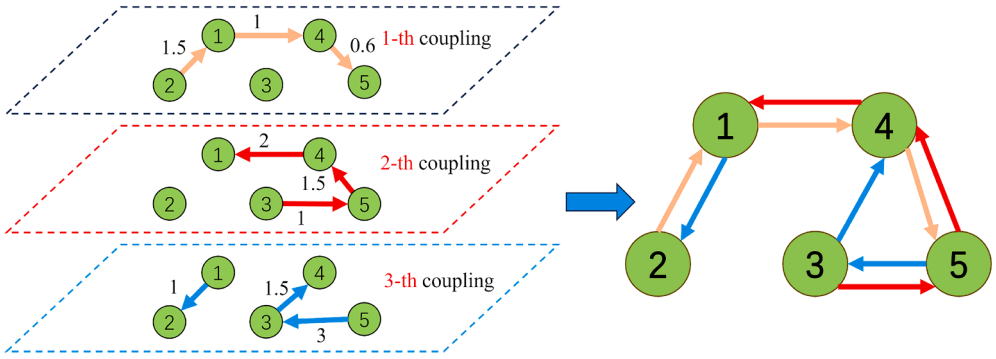


(a) The underlying topology (b) The union coummunication topology

**Fig. 1.** The joint connectivity.

Define the weighted union matrices $\mathcal{G}^{(k)} \in R^{\mathcal{N}\times\mathcal{N}}$ as

$$\mathcal{G}^{(k)} = \sum_{\eta=1}^{\sigma} c^{\eta}\gamma_k^{\eta} G^{\eta}, \quad k \in \overline{1,n}.$$

**Assumption 3.** The communication topology of $\mathcal{G}^{(k)}$ is strong connected for $k \in \overline{1,n}$.

**Remark 2.** In the existing researches on RDNNs with multiweighted coupling [34], it is conventionally assumed that the communication topology of each layer's coupling is strongly connected. However, this study introduces a more relaxed condition. Specifically, only the union communication topology of all coupling layers is required to be connected in Assumption 3, as illustrated in Fig. 1, which is evidently less conservative.

Under Assumption 3, $\mathcal{G}^{(k)}$ has a simple zero eigenvalue and there exists a normalized vector $\xi^{(k)} = (\xi_1^k, \xi_2^k, \dots, \xi_{\mathcal{N}}^k)^T \in \mathcal{R}^{\mathcal{N}}$ with $\xi_m^k > 0$ $(m \in \overline{1,\mathcal{N}})$ satisfying $(\mathcal{G}^{(k)})^T\xi^{(k)} = \mathbf{0}_{\mathcal{N}}$ and $\sum_{i=1}^{\mathcal{N}} \xi_i^k = 1$. Based on this, define a virtual target as

$$\bar{z}^k(t,\varsigma) = \sum_{m=1}^{\mathcal{N}} \xi_m^k z_m^k(t,\varsigma), \quad (t,\varsigma) \in \mathcal{R}_{\geq 0} \times (\underline{\alpha}, \overline{\alpha}),$$

where $\bar{z}^k(t,\varsigma) \in \mathcal{R}$, $k \in \overline{1,n}$, and further denote $\varphi^k(t,\varsigma) = \sum_{m=1}^{\mathcal{N}} \xi_m^k \phi_m^k(t,\varsigma)$, $(t,\varsigma) \in [-\iota, 0] \times (\underline{\alpha}, \overline{\alpha})$.

Since $\mathcal{G}^{(k)^T}\xi^{(k)} = \mathbf{0}_{\mathcal{N}}$, $\sum_{\eta=1}^{\sigma}\sum_{m=1}^{\mathcal{N}} c^{\eta}\gamma_k^{\eta}g_m^{\eta}\xi_m^k = 0$, $m \in \overline{1,\mathcal{N}}$, $k \in \overline{1,n}$, then

$$\begin{aligned}
\frac{\partial \bar{z}^k(t,\varsigma)}{\partial t} &= d_k \frac{\partial^2 \bar{z}^k(t,\varsigma)}{\partial \varsigma^2} - a_k \bar{z}^k(t,\varsigma) + \sum_{m=1}^{\mathcal{N}} \xi_m^k \sum_{s=1}^{n} b_{ks}^1 f_1^s\big(z_m^s(t,\varsigma)\big) \\
&\quad + \sum_{m=1}^{\mathcal{N}} \xi_m^k \sum_{s=1}^{n} b_{ks}^2 f_2^s\big(z_m^s(\varrho(t),\varsigma)\big) + \sum_{m=1}^{\mathcal{N}} \xi_m^k \sum_{s=1}^{n} b_{ks}^3 \int_{t-\iota(t)}^{t} f_3^s\big(z_m^s(\upsilon,\varsigma)\big)\mathrm{d}\upsilon \\
&\quad + \sum_{m=1}^{\mathcal{N}} \xi_m^k \omega_m^k(t,\varsigma) + \sum_{m=1}^{\mathcal{N}} \xi_m^k u_m^k(t,\varsigma).
\end{aligned} \tag{4}$$

Denote the error $e_i^k(t,\varsigma) = z_i^k(t,\varsigma) - \bar{z}^k(t,\varsigma) \in \mathcal{R}$, it follows from systems (3) and (4) that

$$\begin{aligned}
\frac{\partial e_i^k(t,\varsigma)}{\partial t} &= d_k \frac{\partial^2 e_i^k(t,\varsigma)}{\partial \varsigma^2} - a_k e_i^k(t,\varsigma) \\
&\quad + \sum_{s=1}^{n} b_{ks}^1 f_1^s\big(z_i^s(t,\varsigma)\big) - \sum_{m=1}^{\mathcal{N}} \xi_m^k \sum_{s=1}^{n} b_{ks}^1 f_1^s\big(z_m^s(t,\varsigma)\big) \\
&\quad + \sum_{s=1}^{n} b_{ks}^2 f_2^s\big(z_i^s(\varrho(t),\varsigma)\big) - \sum_{m=1}^{\mathcal{N}} \xi_m^k \sum_{s=1}^{n} b_{ks}^2 f_2^s\big(z_m^s(\varrho(t),\varsigma)\big) \\
&\quad + \sum_{s=1}^{n} b_{ks}^3 \int_{t-\iota(t)}^{t} f_3^s\big(z_i^s(\upsilon,\varsigma)\big)\mathrm{d}\upsilon - \sum_{m=1}^{\mathcal{N}} \xi_m^k \sum_{s=1}^{n} b_{ks}^3 \int_{t-\iota(t)}^{t} f_3^s\big(z_m^s(\upsilon,\varsigma)\big)\mathrm{d}\upsilon \\
&\quad + \omega_i^k(t,\varsigma) - \sum_{m=1}^{\mathcal{N}} \xi_m^k \omega_m^k(t,\varsigma) + u_i^k(t,\varsigma) - \sum_{m=1}^{\mathcal{N}} \xi_m^k u_m^k(t,\varsigma)
\end{aligned}$$

$$+\sum_{\eta=1}^{\sigma}\sum_{j=1}^{\mathcal{N}} c^{\eta} g_{ij}^{\eta}\gamma_k^{\eta} z_j^k(t,\varsigma), \quad i\in\overline{1,\mathcal{N}}, k\in\overline{1,n}. \tag{5}$$

To explore the passivity of system (5), its output is given as

$$y_i(t,\varsigma)=Pe_i(t,\varsigma)+Q\bar{\omega}_i(t,\varsigma), \quad i\in\overline{1,\mathcal{N}}, \tag{6}$$

where $y_i(t,\varsigma)=(y_i^1(t,\varsigma),\dots,y_i^p(t,\varsigma))^T\in\mathcal{R}^p$, $e_i(t,\varsigma)=(e_i^1(t,\varsigma),\dots,e_i^n(t,\varsigma))^T\in\mathcal{R}^n$, $\bar{\omega}_i(t,\varsigma)=(\bar{\omega}_i^1(t,\varsigma),\dots,\bar{\omega}_i^n(t,\varsigma))^T\in\mathcal{R}^n$, $\bar{\omega}_i^k(t,\varsigma)=\omega_i^k(t,\varsigma)-\sum_{m=1}^{\mathcal{N}}\xi_m^k\omega_m^k(t,\varsigma)$, and $P,Q\in\mathcal{R}^{p\times n}$.

Define

$$\hat{\omega}(t,\varsigma)=\left(\left(\hat{\omega}^{(1)}(t,\varsigma)\right)^T,\left(\hat{\omega}^{(2)}(t,\varsigma)\right)^T,\dots,\left(\hat{\omega}^{(n)}(t,\varsigma)\right)^T\right)^T\in\mathcal{R}^{n\mathcal{N}},$$
$$\hat{\omega}^{(k)}(t,\varsigma)=(\bar{\omega}_1^k(t,\varsigma),\bar{\omega}_2^k(t,\varsigma),\dots,\bar{\omega}_{\mathcal{N}}^k(t,\varsigma))^T\in\mathcal{R}^{\mathcal{N}},$$
$$\hat{y}(t,\varsigma)=\left(\left(y^{(1)}(t,\varsigma)\right)^T,\left(y^{(2)}(t,\varsigma)\right)^T,\dots,\left(y^{(1)}(t,\varsigma)\right)^T\right)^T\in\mathcal{R}^{p\mathcal{N}},$$
$$y^{(k)}(t,\varsigma)=(y_1^k(t,\varsigma),y_2^k(t,\varsigma),\dots,y_{\mathcal{N}}^k(t,\varsigma))^T\in\mathcal{R}^{\mathcal{N}}.$$

**Definition 1.** [25]. System (5) with input vector $\hat{\omega}(t,\varsigma)\in\mathcal{R}^{n\mathcal{N}}$ and output vector $\hat{y}(t,\varsigma)\in\mathcal{R}^{p\mathcal{N}}$ is said to be strictly passive if there exist a non-negative storage function $V(t)$ and matrices $\mathcal{H}\in\mathcal{R}^{p\mathcal{N}\times n\mathcal{N}}$, $0<\mathcal{H}_1\in\mathcal{R}^{n\mathcal{N}\times n\mathcal{N}}$, $0<\mathcal{H}_2\in\mathcal{R}^{p\mathcal{N}\times p\mathcal{N}}$ such that for any $t\in\mathcal{R}_{\geq 0}$,

$$\dot{V}(t)\leq\int_{\underline{\alpha}}^{\overline{\alpha}}\hat{y}^T(t,\varsigma)\mathcal{H}\hat{\omega}(t,\varsigma)\mathrm{d}\varsigma-\int_{\underline{\alpha}}^{\overline{\alpha}}\hat{\omega}^T(t,\varsigma)\mathcal{H}_1\hat{\omega}(t,\varsigma)\mathrm{d}\varsigma-\int_{\underline{\alpha}}^{\overline{\alpha}}\hat{y}^T(t,\varsigma)\mathcal{H}_2\hat{y}(t,\varsigma)\mathrm{d}\varsigma.$$

Furthermore, system (5) is said to be passive if $\mathcal{H}_1=\mathbf{0}_{n\mathcal{N}\times n\mathcal{N}}$ and $\mathcal{H}_2=\mathbf{0}_{p\mathcal{N}\times p\mathcal{N}}$. System (5) is input-strictly passive if $\mathcal{H}_1>0$ and $\mathcal{H}_2=\mathbf{0}_{p\mathcal{N}\times p\mathcal{N}}$, system (5) is output-strictly passive if $\mathcal{H}_2>0$ and $\mathcal{H}_1=\mathbf{0}_{n\mathcal{N}\times n\mathcal{N}}$.

**Lemma 1.** *[17]. For any scalar $\varepsilon>0$, vectors $x$ and $y$, then $2x^Ty\leq\varepsilon x^Tx+\varepsilon^{-1}y^Ty$.*

**Lemma 2.** *[41]. For any scalars $x_2>x_1>0$, and a square-integrable vector function $z:[x_1,x_2]\to\mathcal{R}^n$,*

$$\left(\int_{x_1}^{x_2}z(v)\mathrm{d}v\right)^T\left(\int_{x_1}^{x_2}z(v)\mathrm{d}v\right)\leq(x_2-x_1)\int_{x_1}^{x_2}z^T(v)z(v)\mathrm{d}v.$$

**Lemma 3.** *[42]. Assume that $z:[\underline{\alpha},\overline{\alpha}]\to\mathcal{R}^n$ be a square-integrable vector function with $z(\underline{\alpha})=0$ or $z(\overline{\alpha})=0$ and $0<\mathcal{M}\in\mathcal{R}^{n\times n}$, then*

$$\int_{\underline{\alpha}}^{\overline{\alpha}}z(\xi)^T\mathcal{M}z(\xi)\mathrm{d}\xi\leq\frac{4(\overline{\alpha}-\underline{\alpha})^2}{\pi^2}\int_{\underline{\alpha}}^{\overline{\alpha}}\left(\frac{\mathrm{d}z}{\mathrm{d}\xi}\right)^T\mathcal{M}\left(\frac{\mathrm{d}z}{\mathrm{d}\xi}\right)\mathrm{d}\xi.$$

*Moreover, if $z(\underline{\alpha})=z(\overline{\alpha})=0$, then*

$$\int_{\underline{\alpha}}^{\overline{\alpha}}z(\xi)^T\mathcal{M}z(\xi)\mathrm{d}\xi\leq\frac{(\overline{\alpha}-\underline{\alpha})^2}{\pi^2}\int_{\underline{\alpha}}^{\overline{\alpha}}\left(\frac{\mathrm{d}z}{\mathrm{d}\xi}\right)^T\mathcal{M}\left(\frac{\mathrm{d}z}{\mathrm{d}\xi}\right)\mathrm{d}\xi.$$

## 3. Main results

In this section, the passivity and synchronization for RDNNs are investigated by designing the spatial sampling controller.

For the convenience of subsequent analysis, denote $\mathcal{P}=P\otimes\mathbf{I}_{\mathcal{N}}$, $\mathcal{Q}=Q\otimes\mathbf{I}_{\mathcal{N}}$, $\Lambda^{(k)}=\mathrm{diag}\{\xi_1^k,\xi_2^k,\dots,\xi_{\mathcal{N}}^k\}$, $\Lambda=\mathrm{diag}\{\Lambda^{(1)},\Lambda^{(2)},\dots,\Lambda^{(n)}\}\in\mathcal{R}^{n\mathcal{N}\times n\mathcal{N}}$, $\rho=1-\frac{\varepsilon_4}{2}-\frac{\delta^2}{2\varepsilon_4(\overline{\alpha}-\underline{\alpha})^2}$, $\mathcal{G}=\mathrm{diag}\{\mathcal{G}^{(1)},\mathcal{G}^{(2)},\dots,\mathcal{G}^{(n)}\}\in\mathcal{R}^{n\mathcal{N}\times n\mathcal{N}}$, and

$$\Psi=\Lambda\mathcal{G}-\Lambda\left\{\left[\frac{\pi^2}{(\overline{\alpha}-\underline{\alpha})^2}D+\mathcal{A}-\sum_{r=1}^{3}\frac{\mathcal{B}_r\mathcal{B}_r^T}{2\varepsilon_r}-\left(\frac{\varepsilon_1L_1}{2}+\frac{\varepsilon_2L_2}{2\hat{\rho}}+\frac{\varepsilon_3L_3\bar{l}^2}{2}\right)\mathbf{I}_n\right]\otimes\mathbf{I}_{\mathcal{N}}\right\}-\rho\Lambda\varpi.$$

### 3.1. Passivity for RDNNs

First of all, we consider the passivity of system (5) by designing a kind of sampled-data control strategy, the control architecture is shown in Fig. 2. A set of fixed points $\varsigma_p$ is placed such that $\underline{\alpha}=\varsigma_0<\varsigma_1<\cdots<\varsigma_{m-1}<\varsigma_m=\overline{\alpha}$, $[\varsigma_p,\varsigma_{p+1})$ represents the sampling interval and satisfies $\sup_{p\in\overline{0,m-1}}\{\varsigma_{p+1}-\varsigma_p\}=\delta$, $\bar{\varsigma}_p=\frac{\varsigma_p+\varsigma_{p+1}}{2}$ is the sampling point.

To realize the passivity of system (5), $m$ sensors are placed on the midpoint of each sample subintervals $[\varsigma_p,\varsigma_{p+1})$ and the controller is designed as

$$u_i(t,\varsigma)=-\varpi_ie_i(t,\bar{\varsigma}_p), \quad \varsigma\in[\varsigma_p,\varsigma_{p+1}), \quad p\in\overline{0,m-1}, \tag{7}$$

where $t\in\mathcal{R}_{\geq 0}$, $\varpi=\mathbf{I}_n\otimes\mathrm{diag}\{\varpi_1,\varpi_2,\dots,\varpi_{\mathcal{N}}\}$, $\varpi_i$ is the control gain.

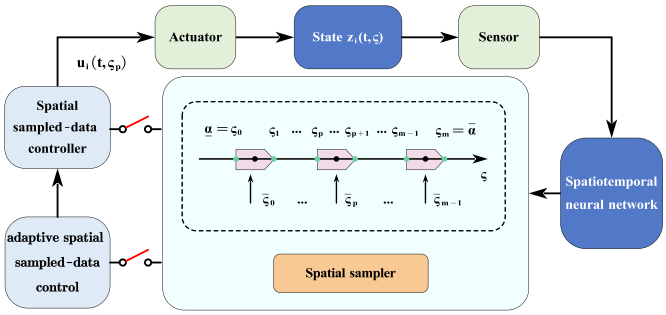


**Fig. 2.** Spatial sampling control architecture.

**Remark 3.** The spatial sampling controller (7) proposed in this paper operates only at key positions within the spatial region. It offers two main advantages. Economically, compared to the full-domain controllers in [25–27], it avoids resource waste caused by deploying control nodes throughout the entire space. Technically, this sampling mode relies on the in-depth analysis of spatial characteristics. For example, in intelligent transportation systems, the installation of traffic signals and surveillance equipment ensures efficient city-wide traffic management.

**Theorem 1.** *Under Assumptions 1–3 and spatial sampling controller (7), system (5) is strictly passive if there exist scalars* $\varepsilon_i > 0$ $(i \in \overline{1,4})$, *matrix* $\mathcal{H}$, *positive-definite matrices* $\mathcal{H}_1$ *and* $\mathcal{H}_2$ *such that*

$$C_1: \quad \Xi = \begin{pmatrix} \Upsilon & \Sigma \\ \Sigma^T & \Delta \end{pmatrix} \le 0,$$

$$C_2: \quad \frac{\delta^2}{2\varepsilon_4 \pi^2} \varpi - D \otimes \boldsymbol{I}_{\mathcal{N}} \le 0,$$

*where* $\Upsilon = [\Psi - \mathcal{P}^T \mathcal{H}_2 \mathcal{P}]^s$, $\Sigma = \frac{1}{2}\Lambda + \mathcal{P}^T [\mathcal{H}_2]^s \mathcal{Q} - \frac{1}{2}\mathcal{P}^T \mathcal{H}$, $\Delta = \mathcal{Q}^T [\mathcal{H}_2]^s \mathcal{Q} + [\mathcal{H}_1]^s - [\mathcal{Q}^T \mathcal{H}]^s$.

**Proof.** Pick a Lyapunov functional

$$V(t) = \mathcal{U}(t) + \eta_1 \int_{\varrho(t)}^{t} \mathcal{U}(v)\mathrm{d}v + \eta_2 \int_{-\bar{\iota}}^{0} \left[ \int_{t+\theta}^{t} \mathcal{U}(v)\mathrm{d}v \right] \mathrm{d}\theta,$$

and

$$\mathcal{U}(t) = \frac{1}{2} \sum_{k=1}^{n} \int_{\underline{\alpha}}^{\overline{\alpha}} \left( e^{(k)}(t,\varsigma) \right)^T \Lambda^{(k)} e^{(k)}(t,\varsigma)\mathrm{d}\varsigma,$$

where $t \in \mathcal{R}_{\ge 0}$, $\eta_1 = \frac{\varepsilon_2 L_2}{\hat{o}}$, $\eta_2 = \varepsilon_3 L_3 \bar{\iota}$, $e^{(k)} = (e_1^k(t,\varsigma), \dots, e_{\mathcal{N}}^k(t,\varsigma))^T$, $k \in \overline{1,n}$, $\hat{e}(t,\varsigma) = \left( \left(e^{(1)}(t,\varsigma)\right)^T, \left(e^{(2)}(t,\varsigma)\right)^T, \dots, \left(e^{(n)}(t,\varsigma)\right)^T \right)^T \in \mathcal{R}^{n\mathcal{N}}$.

Take the derivative to $\mathcal{U}(t)$ along with error system (5),

$$\begin{aligned}
\dot{\mathcal{U}}(t) = & \sum_{i=1}^{\mathcal{N}} \sum_{k=1}^{n} \int_{\underline{\alpha}}^{\overline{\alpha}} \xi_i^k e_i^k(t,\varsigma) \Big[ d_k \frac{\partial^2 e_i^k(t,\varsigma^2)}{\partial \varsigma} - a_k e_i^k(t,\varsigma) \\
& + \sum_{s=1}^{n} b_{ks}^1 f_1^s(z_i^s(t,\varsigma)) - \sum_{s=1}^{n} b_{ks}^1 f_1^s(\bar{z}^s(t,\varsigma)) \\
& + \sum_{s=1}^{n} b_{ks}^1 f_1^s(\bar{z}^s(t,\varsigma)) - \sum_{m=1}^{\mathcal{N}} \xi_m^k \sum_{s=1}^{n} b_{ks}^1 f_1^s(z_m^s(t,\varsigma)) \\
& + \sum_{s=1}^{n} b_{ks}^2 f_2^s(z_i^s(\varrho(t),\varsigma)) - \sum_{s=1}^{n} b_{ks}^2 f_2^s(\bar{z}^s(\varrho(t),\varsigma)) \\
& + \sum_{s=1}^{n} b_{ks}^2 f_2^s(\bar{z}_i^s(\varrho(t),\varsigma) - \sum_{m=1}^{\mathcal{N}} \xi_m^k \sum_{s=1}^{n} b_{ks}^2 f_2^s(z_m^s(\varrho(t),\varsigma) \\
& + \sum_{s=1}^{n} b_{ks}^3 \int_{t-\iota(t)}^{t} f_3^s(z_i^s(v,\varsigma))\mathrm{d}v - \sum_{s=1}^{n} b_{ks}^3 \int_{t-\iota(t)}^{t} f_3^s(\bar{z}^s(v,\varsigma))\mathrm{d}v \\
& + \sum_{s=1}^{n} b_{ks}^3 \int_{t-\iota(t)}^{t} f_3^s(\bar{z}^s(v,\varsigma))\mathrm{d}v - \sum_{m=1}^{\mathcal{N}} \xi_m^k \sum_{s=1}^{n} b_{ks}^3 \int_{t-\iota(t)}^{t} f_3^s(z_i^s(v,\varsigma))\mathrm{d}v \\
& + \sum_{\eta=1}^{\sigma} \sum_{j=1}^{\mathcal{N}} c^\eta g_{ij}^\eta \gamma_k^\eta z_j^k(t,\varsigma) + \bar{\omega}_i^k(t,\varsigma) + u_i^k(t,\varsigma) - \sum_{m=1}^{\mathcal{N}} \xi_m^k u_m^k(t,\varsigma) \Big] \mathrm{d}\varsigma.
\end{aligned} \tag{8}$$

According to the Dirichlet boundary condition and utilizing integration by parts,

$$\begin{aligned}
&\sum_{i=1}^{\mathcal{N}}\sum_{k=1}^{n}\xi_i^k\int_{\underline{\alpha}}^{\overline{\alpha}}e_i^k(t,\varsigma)d_k\frac{\partial^2 e_i^k(t,\varsigma)}{\partial\varsigma^2}\mathrm{d}\varsigma\\
=&\sum_{i=1}^{\mathcal{N}}\sum_{k=1}^{n}e_i^k\xi_i^k d_k\frac{\partial e_i^k(t,\varsigma)}{\partial\varsigma}\Big|_{\underline{\alpha}}^{\overline{\alpha}}-\sum_{i=1}^{\mathcal{N}}\sum_{k=1}^{n}\int_{\underline{\alpha}}^{\overline{\alpha}}\frac{\partial e_i^k(t,\varsigma)}{\partial\varsigma}\xi_i^k d_k\frac{\partial e_i^k(t,\varsigma)}{\partial\varsigma}\mathrm{d}\varsigma\\
=&-\sum_{k=1}^{n}\int_{\underline{\alpha}}^{\overline{\alpha}}d_k\Big(\frac{\partial e^{(k)}(t,\varsigma)}{\partial\varsigma}\Big)^T\Lambda^{(k)}\Big(\frac{\partial e^{(k)}(t,\varsigma)}{\partial\varsigma}\Big)\mathrm{d}\varsigma\\
=&-\int_{\underline{\alpha}}^{\overline{\alpha}}\Big(\frac{\partial\hat{e}(t,\varsigma)}{\partial\varsigma}\Big)^T\Lambda(\mathcal{D}\otimes\mathbf{I}_{\mathcal{N}})\Big(\frac{\partial\hat{e}(t,\varsigma)}{\partial\varsigma}\Big)\mathrm{d}\varsigma.
\end{aligned}\tag{9}$$

It is noted that

$$\sum_{i=1}^{\mathcal{N}}\xi_i^k e_i^k(t,\varsigma)=\sum_{i=1}^{\mathcal{N}}\xi_i^k\Big[z_i^k(t,\varsigma)-\sum_{m=1}^{\mathcal{N}}\xi_m^k z_m^k(t,\varsigma)\Big]=0,$$

which shows that

$$\begin{aligned}
&\sum_{i=1}^{\mathcal{N}}\sum_{k=1}^{n}\xi_i^k e_i^k(t,\varsigma)\Big[\sum_{s=1}^{n}b_{ks}^1 f_1^s(\bar{z}^s(t,\varsigma))-\sum_{m=1}^{\mathcal{N}}\xi_m^k\sum_{s=1}^{n}b_{ks}^1 f_1^s(z_m^s(t,\varsigma))\Big]=0,\\
&\sum_{i=1}^{\mathcal{N}}\sum_{k=1}^{n}\xi_i^k e_i^k(t,\varsigma)\Big[\sum_{s=1}^{n}b_{ks}^2 f_2^s(\bar{z}^s(\varrho(t),\varsigma))-\sum_{m=1}^{\mathcal{N}}\xi_m^k\sum_{s=1}^{n}b_{ks}^2 f_2^s(z_m^s(\varrho(t),\varsigma))\Big]=0,\\
&\sum_{i=1}^{\mathcal{N}}\sum_{k=1}^{n}\xi_i^k e_i^k(t,\varsigma)\int_{t-\iota(t)}^{t}\Big[\sum_{s=1}^{n}b_{ks}^3 f_3^s(\bar{z}^s(v,\varsigma))-\sum_{m=1}^{\mathcal{N}}\xi_m^k\sum_{s=1}^{n}b_{ks}^3 f_3^s(z_m^s(v,\varsigma))\Big]\mathrm{d}v=0,\\
&\sum_{i=1}^{\mathcal{N}}\sum_{k=1}^{n}\xi_i^k e_i^k(t,\varsigma)\Big[\sum_{m=1}^{\mathcal{N}}\xi_m^k u_m^k(t,\varsigma)\Big]=0.
\end{aligned}$$

Define

$$\begin{aligned}
&\tilde{e}_i(t,\varsigma)=\mathrm{diag}\{\sqrt{\xi_i^n},\dots,\sqrt{\xi_i^n}\}e_i(t,\varsigma)\in\mathcal{R}^n,\\
&\tilde{F}_r(e_i(\cdot,\varsigma))=\mathrm{diag}\{\sqrt{\xi_i^n},\dots,\sqrt{\xi_i^n}\}(f_r(z_i(\cdot,\varsigma))-f_r(\bar{z}(\cdot,\varsigma)))\in\mathcal{R}^n.
\end{aligned}$$

From Assumption 1, Lemmas 1 and 2, there exist some positive scalars $\varepsilon_i$ ($i\in\overline{1,3}$) such that

$$\begin{aligned}
&\sum_{k=1}^{n}e_i^k(t,\varsigma)\xi_i^k\sum_{s=1}^{n}b_{ks}^1\Big[f_1^s(z_i^s(t,\varsigma))-f_1^s(\bar{z}^s(t,\varsigma))\Big]\\
&+\sum_{k=1}^{n}e_i^k(t,\varsigma)\xi_i^k\sum_{s=1}^{n}b_{ks}^2\Big[f_2^s(z_i^s(\varrho(t),\varsigma))-f_2^s(\bar{z}^s(\varrho(t),\varsigma))\Big]\\
&+\sum_{k=1}^{n}e_i^k(t,\varsigma)\xi_i^k\sum_{s=1}^{n}b_{ks}^3\int_{t-\iota(t)}^{t}\Big[f_3^s(z_i^s(v,\varsigma))-f_3^s(\bar{z}^s(v,\varsigma))\Big]\mathrm{d}v\\
\le&\frac{1}{2\varepsilon_1}\sum_{i=1}^{\mathcal{N}}\tilde{e}_i^T(t,\varsigma)\mathcal{B}_1\mathcal{B}_1^T\tilde{e}_i(t,\varsigma)+\frac{\varepsilon_1 L_1}{2}\sum_{i=1}^{\mathcal{N}}\tilde{e}_i^T(t,\varsigma)\tilde{e}_i(t,\varsigma)\\
&+\frac{1}{2\varepsilon_2}\sum_{i=1}^{\mathcal{N}}\tilde{e}_i^T(t,\varsigma)\mathcal{B}_2\mathcal{B}_2^T\tilde{e}_i(t,\varsigma)+\frac{\varepsilon_2 L_2}{2}\sum_{i=1}^{\mathcal{N}}\tilde{e}_i^T(\varrho(t),\varsigma)\tilde{e}_i(\varrho(t),\varsigma)\\
&+\frac{1}{2\varepsilon_3}\sum_{i=1}^{\mathcal{N}}\tilde{e}_i^T(t,\varsigma)\mathcal{B}_3\mathcal{B}_3^T\tilde{e}_i(t,\varsigma)+\frac{\varepsilon_3 L_3\bar{\iota}}{2}\sum_{i=1}^{\mathcal{N}}\int_{t-\iota(t)}^{t}\tilde{e}_i^T(v,\varsigma)\tilde{e}_i(v,\varsigma)\mathrm{d}v\\
\le&\frac{1}{2}\hat{e}^T(t,\varsigma)\Lambda(\sum_{r=1}^{3}\frac{1}{\varepsilon_r}\mathcal{B}_r\mathcal{B}_r^T\otimes\mathbf{I}_{\mathcal{N}})\hat{e}(t,\varsigma)+\frac{\varepsilon_1 L_1}{2}\hat{e}^T(t,\varsigma)\Lambda\hat{e}(t,\varsigma)\\
&+\frac{\varepsilon_2 L_2}{2}\hat{e}^T(\varrho(t),\varsigma)\Lambda\hat{e}(\varrho(t),\varsigma)+\frac{\varepsilon_3 L_3\bar{\iota}}{2}\int_{t-\iota(t)}^{t}\hat{e}^T(v,\varsigma)\Lambda\hat{e}(v,\varsigma)\mathrm{d}v.
\end{aligned}\tag{10}$$

Note that $e_i^k(t,\bar{\varsigma}_p)=e_i^k(t,\varsigma)-\int_{\bar{\varsigma}_p}^{\varsigma}\frac{\partial e_i^k(t,s)}{\partial s}\mathrm{d}s$, $\varsigma_{p+1}-\bar{\varsigma}_p\le\frac{\delta}{2}$ and $\bar{\varsigma}_p-\varsigma_p\le\frac{\delta}{2}$, then

$$\sum_{i=1}^{\mathcal{N}}\sum_{k=1}^{n}\int_{\underline{\alpha}}^{\overline{\alpha}}e_i^k(t,\varsigma)\xi_i^k u_i^k(t,\varsigma)\mathrm{d}\varsigma$$

$$
\begin{aligned}
&= -\int_{\underline{\alpha}}^{\overline{\alpha}} \hat{e}^T(t,\varsigma)\Lambda\varpi\hat{e}(t,\varsigma)\mathrm{d}\varsigma + \int_{\underline{\alpha}}^{\overline{\alpha}} \hat{e}^T(t,\varsigma)\Lambda\varpi\left(\int_{\bar{\varsigma}_p}^{\varsigma}\frac{\partial\hat{e}(t,s)}{\partial s}\mathrm{d}s\right)\mathrm{d}\varsigma\\
&\le -\int_{\underline{\alpha}}^{\overline{\alpha}} \hat{e}^T(t,\varsigma)\Lambda\varpi\hat{e}(t,\varsigma)\mathrm{d}\varsigma + \sum_{p=0}^{m-1}\frac{\varepsilon_4}{2}\int_{x_p}^{x_{p+1}} \hat{e}^T(t,\varsigma)\Lambda\varpi\hat{e}(t,\varsigma)\,\mathrm{d}\varsigma\\
&\quad + \frac{1}{2\varepsilon_4}\sum_{p=0}^{m-1}\int_{\varsigma_p}^{\varsigma_{p+1}}\left(\hat{e}(t,\varsigma)-\hat{e}(t,\bar{\varsigma}_p)\right)^T\Lambda\varpi\left(\hat{e}(t,\varsigma)-\hat{e}(t,\bar{\varsigma}_p)\right)\mathrm{d}\varsigma\\
&= -\int_{\underline{\alpha}}^{\overline{\alpha}} \hat{e}^T(t,\varsigma)\Lambda\varpi\hat{e}(t,\varsigma)\mathrm{d}\varsigma + \frac{\varepsilon_4}{2}\sum_{p=0}^{m-1}\int_{\varsigma_p}^{\varsigma_{p+1}} \hat{e}^T(t,\varsigma)\Lambda\varpi\hat{e}(t,\varsigma)\mathrm{d}\varsigma\\
&\quad + \frac{1}{2\varepsilon_4}\sum_{p=0}^{m-1}\left[\int_{\varsigma_p}^{\bar{\varsigma}_p}\left(\hat{e}(t,\varsigma)-\hat{e}(t,\bar{\varsigma}_p)\right)^T\Lambda\varpi\left(\hat{e}(t,\varsigma)-\hat{e}(t,\bar{\varsigma}_p)\right)\mathrm{d}\varsigma\right.\\
&\quad \left. + \int_{\bar{\varsigma}_p}^{\varsigma_{p+1}}\left(\hat{e}(t,\varsigma)-\hat{e}(t,\bar{\varsigma}_p)\right)^T\Lambda\varpi\left(\hat{e}(t,\varsigma)-\hat{e}(t,\bar{\varsigma}_p)\right)\mathrm{d}\varsigma\right]\\
&\le -(1-\frac{\varepsilon_4}{2})\int_{\underline{\alpha}}^{\overline{\alpha}} \hat{e}^T(t,\varsigma)\Lambda\varpi\hat{e}(t,\varsigma)\mathrm{d}\varsigma\\
&\quad + \frac{1}{2\varepsilon_4}\sum_{p=0}^{m-1}\left[\frac{4(\bar{\varsigma}_p-\varsigma_p)^2}{\pi^2}\int_{\varsigma_p}^{\bar{\varsigma}_p}\left(\frac{\partial\hat{e}(t,\varsigma)}{\partial\varsigma}\right)^T\Lambda\varpi\frac{\partial\hat{e}(t,\varsigma)}{\partial\varsigma}\mathrm{d}\varsigma\right.\\
&\quad \left. + \frac{4(\varsigma_{p+1}-\bar{\varsigma}_p)^2}{\pi^2}\int_{\bar{\varsigma}_p}^{\varsigma_{p+1}}\left(\frac{\partial\hat{e}(t,\varsigma)}{\partial\varsigma}\right)^T\Lambda\varpi\frac{\partial\hat{e}(t,\varsigma)}{\partial\varsigma}\mathrm{d}\varsigma\right]\\
&\le -(1-\frac{\varepsilon_4}{2})\int_{\underline{\alpha}}^{\overline{\alpha}} \hat{e}^T(t,\varsigma)\Lambda\varpi\hat{e}(t,\varsigma)\mathrm{d}\varsigma\\
&\quad + \frac{\delta^2}{2\varepsilon_4\pi^2}\int_{\underline{\alpha}}^{\overline{\alpha}}\left(\frac{\partial\hat{e}(t,\varsigma)}{\partial\varsigma}\right)^T\Lambda\varpi\frac{\partial\hat{e}(t,\varsigma)}{\partial\varsigma}\mathrm{d}\varsigma.
\end{aligned}
\tag{11}
$$

According to the condition $C_2$, Eq. (9), inequality (11) and Lemma 3,

$$
\begin{aligned}
&-\int_{\underline{\alpha}}^{\overline{\alpha}}\frac{\partial\hat{e}^T(t,\varsigma)}{\partial\varsigma}\Lambda\left[D\otimes\mathbf{I}_{\mathcal{N}}-\frac{\delta^2}{2\varepsilon_4\pi^2}\varpi\right]\frac{\partial\hat{e}(t,\varsigma)}{\partial\varsigma}\mathrm{d}\varsigma\\
&\le -\frac{1}{(\overline{\alpha}-\underline{\alpha})^2}\int_{\underline{\alpha}}^{\overline{\alpha}}\hat{e}^T(t,\varsigma)\Lambda\left[\pi^2D\otimes\mathbf{I}_{\mathcal{N}}-\frac{\delta^2}{2\varepsilon_4}\varpi\right]\hat{e}(t,\varsigma)\mathrm{d}\varsigma.
\end{aligned}
\tag{12}
$$

Substituting the formulas (9)–(12) into the Eq. (8) yields that

$$
\begin{aligned}
\dot{\mathcal{U}}(t) \le &\int_{\underline{\alpha}}^{\overline{\alpha}}\hat{e}^T(t,\varsigma)\left\{[\Lambda\mathcal{G}]^s-\Lambda\left[\left(\frac{\pi^2}{(\overline{\alpha}-\underline{\alpha})^2}\mathcal{D}+\mathcal{A}-\sum_{r=1}^{3}\frac{\mathcal{B}_r\mathcal{B}_r^T}{2\varepsilon_r}-\frac{\varepsilon_1L_1}{2}\mathbf{I}_n\right)\otimes\mathbf{I}_{\mathcal{N}}\right]\right.\\
&\left.-\left(1-\frac{\varepsilon_4}{2}-\frac{\delta^2}{2\varepsilon_4(\overline{\alpha}-\underline{\alpha})^2}\right)\Lambda\varpi\right\}\hat{e}(t,\varsigma)\mathrm{d}\varsigma+\frac{\varepsilon_2L_2}{2}\int_{\underline{\alpha}}^{\overline{\alpha}}\hat{e}^T(\varrho(t),\varsigma)\Lambda\hat{e}(\varrho(t),\varsigma)\mathrm{d}\varsigma\\
&+\frac{\varepsilon_3L_3\bar{\imath}}{2}\int_{\underline{\alpha}}^{\overline{\alpha}}\int_{t-\imath(t)}^{t}\hat{e}^T(v,\varsigma)\Lambda\hat{e}(v,\varsigma)\mathrm{d}v\mathrm{d}\varsigma+\int_{\underline{\alpha}}^{\overline{\alpha}}\hat{e}^T(t,\varsigma)\Lambda\hat{\omega}(t,\varsigma)\mathrm{d}\varsigma.
\end{aligned}
\tag{13}
$$

Combining inequality (13) and Assumption 2,

$$
\begin{aligned}
\dot{V}(t) =&\dot{\mathcal{U}}(t)+\eta_1\mathcal{U}(t)-\eta_1\dot{\varrho}(t)\mathcal{U}(\varrho(t))+\eta_2\left(\bar{\imath}\mathcal{U}(t)-\int_{t-\bar{\imath}}^{t}\mathcal{U}(v)\mathrm{d}v\right)\\
\le &\int_{\underline{\alpha}}^{\overline{\alpha}}\hat{e}^T(t,\varsigma)\left\{[\Lambda\mathcal{G}]^s-\Lambda\left[\left(\frac{\pi^2}{(\overline{\alpha}-\underline{\alpha})^2}\mathcal{D}+\mathcal{A}-\frac{1}{2}\sum_{r=1}^{3}\frac{1}{\varepsilon_r}\mathcal{B}_r\mathcal{B}_r^T\right.\right.\right.\\
&\left.\left.\left.-\frac{\varepsilon_1L_1+\eta_1+\eta_2\bar{\imath}}{2}\mathbf{I}_n\right)\otimes\mathbf{I}_{\mathcal{N}}\right]-\left(1-\frac{\varepsilon_4}{2}-\frac{\delta^2}{2\varepsilon_4(\overline{\alpha}-\underline{\alpha})^2}\right)\Lambda\varpi\right\}\hat{e}(t,\varsigma)\mathrm{d}\varsigma\\
&+\left(\frac{\varepsilon_2L_2}{2}-\frac{\eta_1\dot{\varrho}(t)}{2}\right)\int_{\underline{\alpha}}^{\overline{\alpha}}\hat{e}^T(\varrho(t),\varsigma)\Lambda\hat{e}(\varrho(t),\varsigma)\mathrm{d}\varsigma\\
&+\left(\frac{\varepsilon_3L_3\bar{\imath}}{2}-\frac{\eta_2}{2}\right)\int_{\underline{\alpha}}^{\overline{\alpha}}\int_{t-\imath(t)}^{t}\hat{e}^T(v,\varsigma)\Lambda\hat{e}(v,\varsigma)\mathrm{d}v\mathrm{d}\varsigma
\end{aligned}
$$

$$+\int_{\underline{\alpha}}^{\overline{\alpha}}\hat{e}^T(t,\varsigma)\Lambda\hat{\omega}(t,\varsigma)\mathrm{d}\varsigma$$
$$\leq\int_{\underline{\alpha}}^{\overline{\alpha}}\hat{e}^T(t,\varsigma)\Psi\hat{e}(t,\varsigma)\mathrm{d}\varsigma+\int_{\underline{\alpha}}^{\overline{\alpha}}\hat{e}^T(t,\varsigma)\Lambda\hat{\omega}(t,\varsigma)\mathrm{d}\varsigma.$$

Furthermore, according to Definition 1, one obtains

$$\begin{aligned}
&\dot{V}(t)-\int_{\underline{\alpha}}^{\overline{\alpha}}\hat{y}^T(t,\varsigma)\mathcal{H}\hat{\omega}(t,\varsigma)\mathrm{d}\varsigma+\int_{\underline{\alpha}}^{\overline{\alpha}}\hat{\omega}^T(t,\varsigma)\mathcal{H}_1\hat{\omega}(t,\varsigma)\mathrm{d}\varsigma+\int_{\underline{\alpha}}^{\overline{\alpha}}\hat{y}^T(t,\varsigma)\mathcal{H}_2\hat{y}(t,\varsigma)\mathrm{d}\varsigma\\
&\leq\int_{\underline{\alpha}}^{\overline{\alpha}}\hat{e}^T(t,\varsigma)\Big[\Psi-\mathcal{P}^T\mathcal{H}_2\mathcal{P}\Big]^s\hat{e}(t,\varsigma)\mathrm{d}\varsigma\\
&\quad+\int_{\underline{\alpha}}^{\overline{\alpha}}\hat{e}^T(t,\varsigma)\Big(\frac{1}{2}\Lambda+\mathcal{P}^T[\mathcal{H}_2]^s\mathcal{Q}-\frac{1}{2}\mathcal{P}^T\mathcal{H}\Big)\hat{\omega}(t,\varsigma)\mathrm{d}\varsigma\\
&\quad+\int_{\underline{\alpha}}^{\overline{\alpha}}\hat{\omega}^T(t,\varsigma)\Big(\frac{1}{2}\Lambda+\mathcal{Q}^T[\mathcal{H}_2]^s\mathcal{P}-\frac{1}{2}\mathcal{H}^T\mathcal{P}\Big)\hat{e}(t,\varsigma)\mathrm{d}\varsigma\\
&\quad+\int_{\underline{\alpha}}^{\overline{\alpha}}\hat{\omega}^T(t,\varsigma)\mathrm{d}\varsigma\Big(\mathcal{Q}^T[\mathcal{H}_2]^s\mathcal{Q}+[\mathcal{H}_1]^s-[\mathcal{Q}^T\mathcal{H}]^s\Big)\hat{\omega}(t,\varsigma)\mathrm{d}\varsigma\\
&=\int_{\underline{\alpha}}^{\overline{\alpha}}\mathbf{E}^T(t,\varsigma)\Xi\mathbf{E}(t,\varsigma)\mathrm{d}\varsigma,
\end{aligned}\tag{14}$$

where $\mathbf{E}(t,\varsigma)=(\hat{e}^T(t,\varsigma),\hat{\omega}^T(t,\varsigma))^T$.

By combining the condition $C_1$ and inequality (14),

$$\dot{V}(t)\leq\int_{\underline{\alpha}}^{\overline{\alpha}}\hat{y}^T(t,\varsigma)\mathcal{H}\hat{\omega}(t,\varsigma)\mathrm{d}\varsigma-\int_{\underline{\alpha}}^{\overline{\alpha}}\hat{\omega}^T(t,\varsigma)\mathcal{H}_1\hat{\omega}(t,\varsigma)\mathrm{d}\varsigma-\int_{\underline{\alpha}}^{\overline{\alpha}}\hat{y}^T(t,\varsigma)\mathcal{H}_2\hat{y}(t,\varsigma)\mathrm{d}\varsigma.$$

The proof is finished. □

**Corollary 1.** *Under Assumptions 1–3 and spatial sampled-data controller (7), the error system (5) is input-strictly passive if there exist scalars* $\varepsilon_i>0$ $(i\in\overline{1,4})$ *and matrices* $\mathcal{H}\in\mathcal{R}^{p\mathcal{N}\times n\mathcal{N}}$ *and* $0<\mathcal{H}_1\in\mathcal{R}^{n\mathcal{N}\times n\mathcal{N}}$ *such that*

$$\tilde{\Xi}=\begin{pmatrix}[\Psi]^s & \tilde{\Sigma}\\ \tilde{\Sigma}^T & \tilde{\Delta}\end{pmatrix}\leq 0,\quad \frac{\delta^2}{2\varepsilon_4\pi^2}\varpi-\mathcal{D}\otimes\mathbf{I}_{\mathcal{N}}\leq 0,$$

*where* $\tilde{\Sigma}=\frac{1}{2}\Lambda-\frac{1}{2}\mathcal{P}^T\mathcal{H}$, $\tilde{\Delta}=[\mathcal{H}_1]^s-[\mathcal{Q}^T\mathcal{H}]^s$.

**Corollary 2.** *Under Assumptions 1–3 and spatial sampled-data controller (7), the error system (5) is output-strictly passive if there exist scalars* $\varepsilon_i>0$ $(i\in\overline{1,4})$ *and matrices* $\mathcal{H}\in\mathcal{R}^{p\mathcal{N}\times n\mathcal{N}}$ *and* $0<\mathcal{H}_2\in\mathcal{R}^{p\mathcal{N}\times p\mathcal{N}}$ *such that*

$$\hat{\Xi}=\begin{pmatrix}\Upsilon & \Sigma\\ \Sigma^T & \hat{\Delta}\end{pmatrix}\leq 0,\quad \frac{\delta^2}{2\varepsilon_4\pi^2}\varpi-\mathcal{D}\otimes\mathbf{I}_{\mathcal{N}}\leq 0,$$

*where* $\hat{\Delta}=\mathcal{Q}^T[\mathcal{H}_2]^s\mathcal{Q}-[\mathcal{Q}^T\mathcal{H}]^s$.

**Remark 4.** The established conditions in Theorem 1 depend on the control parameters $\varpi_i$ $(i\in\overline{1,\mathcal{N}})$, the matrices $\mathcal{H}$, $\mathcal{H}1$, $\mathcal{H}_2$, and the free parameters $\varepsilon_1$, $\varepsilon_2$, $\varepsilon_3$, $\varepsilon_4$. By Schur complement Lemma [43], $\Xi\leq 0$ is equivalent to

$$\Delta<0\ \text{ and }\ R-\Sigma\Delta^{-1}\Sigma^T\leq 0.$$

When other parameters are fixed, an increase in the control gain $\varpi_i$ leads to a higher probability of satisfying the condition $\Xi\leq 0$, which implies that the passivity of the error system (5) can be easily ensured by implementing control with large gains. However, it is imperative to avoid large control actions in practice. Therefore, some appropriate free parameters $\varepsilon_r$ $(r\in\overline{1,4})$ can be selected as a tradeoff between convergence performance and control gains. In addition, a decrease in the upper bound of sampling interval $\delta$ facilitates the fulfillment of condition $(C_2)$. The associated parameter selection strategy is presented in Algorithm 1.

**Algorithm 1** The Parameter Selection Strategy in Theorem 1, Corollaries 1 and 2.

- ▶ Give initial conditions, topological structure, network parameters
- ▶ Calculate $\varpi,\varepsilon_1,\varepsilon_2,\varepsilon_3,\varepsilon_4,\mathcal{H},\mathcal{H}_1,\mathcal{H}_2$ by LMI toolbox
  - ◇ Ensure $\Xi<0$ and $\frac{\delta^2}{2\varepsilon_4\pi^2}\varpi-\mathcal{D}\otimes\mathbf{I}_{\mathcal{N}}\leq 0$ in case of strict passivity
  - ◇ Ensure $\tilde{\Xi}<0$ and $\frac{\delta^2}{2\varepsilon_4\pi^2}\varpi-\mathcal{D}\otimes\mathbf{I}_{\mathcal{N}}\leq 0$ in case of input-strict passivity
  - ◇ Ensure $\hat{\Xi}<0$ and $\frac{\delta^2}{2\varepsilon_4\pi^2}\varpi-\mathcal{D}\otimes\mathbf{I}_{\mathcal{N}}\leq 0$ in case of output-strict passivity
- ▶ Draw the simulation results

### 3.2. Synchronization for RDNNs

In this part, the asymptotical synchronization of the RDNN (1) is investigated.

**Definition 2.** The RDNN (1) is asymptotically synchronized if

$$\lim_{t\to+\infty}\|e_i(t,\cdot)\|_{[\underline{\alpha},\overline{\alpha}]}=0,\quad i\in\overline{1,\mathcal{N}}.$$

**Theorem 2.** *Under Assumptions 1–3 and spatial sampling controller (7), the RDNN (1) with $\hat{\omega}(t,\varsigma)\equiv \mathbf{0}n\mathcal{N}$ is asymptotically synchronized if the error system (5) is output-strictly passive and $\mathcal{P}^T[\mathcal{H}_2]^s\mathcal{P}>0$.*

**Proof.** Construct the same Lyapunov functional $V(t)$ as Theorem 1. Since error system (5) is output-strict passive,

$$\dot{V}(t)\le\int_{\underline{\alpha}}^{\overline{\alpha}}\hat{y}^T(t,\varsigma)\mathcal{H}\hat{\omega}(t,\varsigma)\mathrm{d}\varsigma-\int_{\underline{\alpha}}^{\overline{\alpha}}\hat{\omega}^T(t,\varsigma)\mathcal{H}_1\hat{\omega}(t,\varsigma)\mathrm{d}\varsigma-\int_{\underline{\alpha}}^{\overline{\alpha}}\hat{y}^T(t,\varsigma)\mathcal{H}_2\hat{y}(t,\varsigma)\mathrm{d}\varsigma.$$

When $\hat{\omega}(t,\varsigma)=\mathbf{0}_{n\mathcal{N}}$, from the output (6),

$$\dot{V}(t)\le-\int_{\underline{\alpha}}^{\overline{\alpha}}\hat{e}^T(t,\varsigma)\mathcal{P}^T[\mathcal{H}_2]^s\mathcal{P}\hat{e}(t,\varsigma)\mathrm{d}\varsigma<0,$$

which ensures that the asymptotical synchronization for the RDNN (1) is realized. □

**Theorem 3.** *Under Assumptions 1–3 and spatial sampling controller (7), the RDNN (1) with $\hat{\omega}(t,\varsigma)\equiv \mathbf{0}n\mathcal{N}$ is asymptotically synchronized if there exist scalars $\varepsilon_i>0$ ($i\in\overline{1,4}$) such that $\Psi<0$ and $\frac{\delta^2}{2\varepsilon_4\pi^2}\varpi-\mathcal{D}\otimes\mathbf{I}_{\mathcal{N}}\le 0$.*

**Proof.** Similar to Theorem 1, from the condition $\Psi<0$,

$$\dot{V}(t)\le\int_{\underline{\alpha}}^{\overline{\alpha}}\hat{e}^T(t,\varsigma)\Psi\hat{e}(t,\varsigma)\mathrm{d}\varsigma<0,$$

which demonstrates that the RDNN (1) is asymptotically synchronized. □

To further reduce the control gain $\varpi$ determined by the condition $(C_1)$ in Theorem 1, there arises a necessity for an adaptive spatial sampled-data control strategy to dynamically adjust the control gain. The adaptive control strategy is designed as

$$\begin{cases}u_i^k(t,\varsigma)=-\varpi_i(t,\varsigma)e_i^k(t,\bar{\varsigma}_p),\\ \frac{\partial\varpi_i(t,\varsigma)}{\partial t}=\delta_i e^{\beta t}\sum\limits_{k=1}^{n}\xi_i^k e_i^k(t,\varsigma)e_i^k(t,\bar{\varsigma}_p),\end{cases}\tag{15}$$

where $i\in\overline{1,\mathcal{N}}$, $\varpi_i(0,\varsigma)\ge 0$, $\bar{\varsigma}_p=\frac{\varsigma_p+\varsigma_{p+1}}{2}$, $\varsigma\in[\varsigma_p,\varsigma_{p+1})$, $p\in\overline{0,m-1}$, $k\in\overline{1,n}$, $\delta_i$ is an arbitrary positive constant and $\beta>0$ is a sufficiently small real number.

**Remark 5.** Among the recent results on adaptive synchronization of RDNNs, such as [16,29,32], the adaptive law corresponding to the control gain $\frac{\partial\varpi_i(t,\varsigma)}{\partial t}=e_i^T(t,\varsigma)e_i(t,\varsigma)$ was designed. However, the aforementioned adaptive law cannot be directly applied to the spatial sampling mechanism. Unlike this method, a new adaptive spatial sampling control scheme (15) is proposed, which integrates spatial sampling control with adaptive control and effectively reduce control costs.

**Theorem 4.** *Under Assumptions 1–3 and the adaptive spatial sampling controller (15), the RDNN (1) with $\hat{\omega}(t,\varsigma)\equiv \mathbf{0}n\mathcal{N}$ is asymptotically synchronized.*

**Proof.** Pick a new Lyapunov functional

$$\mathcal{W}(t)=\mathcal{V}(t)+R(t),\tag{16}$$

where

$$\mathcal{V}(t)=e^{\beta t}\mathcal{U}(t)+\eta_1 e^{\beta\bar{\sigma}}\int_{\rho(t)}^{t}e^{\beta v}\mathcal{U}(v)\mathrm{d}v+\eta_2 e^{\beta\bar{\imath}}\int_{-\bar{\imath}}^{0}\Big[\int_{t+\theta}^{t}e^{\beta v}\mathcal{U}(v)\mathrm{d}v\Big]\mathrm{d}\theta,$$

$$R(t)=\sum_{i=1}^{\mathcal{N}}\frac{1}{2\delta_i}\int_{\underline{\alpha}}^{\overline{\alpha}}\Big(\varpi_i(t,\varsigma)-\varpi_i^*\Big)^2\mathrm{d}\varsigma,$$

here $\eta_1=\frac{\varepsilon_2 L_2}{\hat{\varphi}}$, $\eta_2=\varepsilon_3 L_3\bar{\imath}$, the definition of $\mathcal{U}(t)$ is same as Theorem 1, and $\varpi_i^*>0$ will be determined in subsequent analysis.

In analogy to Theorem 1, based on the controller (15) and $\hat{\omega}(t,\varsigma)\equiv\mathbf{0}n\mathcal{N}$,

$$\begin{aligned}\dot{\mathcal{U}}(t)\le&\int_{\underline{\alpha}}^{\overline{\alpha}}\hat{e}^T(t,\varsigma)\Big\{[\Lambda\mathcal{G}]^s-\Lambda\Big[\Big(\mathcal{A}-\sum_{r=1}^{3}\frac{\mathcal{B}_r\mathcal{B}_r^T}{2\varepsilon_r}-\frac{\varepsilon_1 L_1}{2}\mathbf{I}_n\Big)\otimes\mathbf{I}_{\mathcal{N}}\Big]\Big\}\hat{e}(t,\varsigma)\mathrm{d}\varsigma\\&-\int_{\underline{\alpha}}^{\overline{\alpha}}\Big(\frac{\partial\hat{e}(t,\varsigma)}{\partial\varsigma}\Big)^T\Lambda(\mathcal{D}\otimes\mathbf{I}_{\mathcal{N}})\Big(\frac{\partial\hat{e}(t,\varsigma)}{\partial\varsigma}\Big)\mathrm{d}\varsigma\end{aligned}$$

$$-\sum_{i=1}^{\mathcal{N}}\sum_{k=1}^{n}\int_{\underline{\alpha}}^{\overline{\alpha}} e_i^k(t,\varsigma)\xi_i^k\varpi_i(t,\varsigma)e_i^k(t,\bar{\varsigma}_p)\mathrm{d}\varsigma+\frac{\varepsilon_2 L_2}{2}\int_{\underline{\alpha}}^{\overline{\alpha}}\hat{e}^T(\varrho(t),\varsigma)\Lambda\hat{e}(\varrho(t),\varsigma)\mathrm{d}\varsigma$$
$$+\frac{\varepsilon_3 L_3\bar{\imath}}{2}\int_{\underline{\alpha}}^{\overline{\alpha}}\int_{t-\bar{\imath}(t)}^{t}\hat{e}^T(v,\varsigma)\Lambda\hat{e}(v,\varsigma)\mathrm{d}v\mathrm{d}\varsigma. \tag{17}$$

Then, from Assumption 2, one has $\bar{\varrho}+\varrho(t)\geq t$ and

$$\begin{aligned}\dot{\mathcal{V}}(t)=&\beta e^{\beta t}\mathcal{U}(t)+e^{\beta t}\dot{\mathcal{U}}(t)+\eta_1 e^{\beta(\bar{\varrho}+t)}\mathcal{U}(t)-\eta_1 e^{\beta(\bar{\varrho}+\varrho(t))}\mathcal{U}(\varrho(t))\dot{\varrho}(t)\\&+\eta_2\bar{\imath}e^{\beta\bar{\imath}}e^{\beta t}\mathcal{U}(t)-\eta_2 e^{\beta t}\int_{-\bar{\imath}}^{0}e^{\beta(\bar{\imath}+\theta)}\mathcal{U}(t+\theta)\mathrm{d}\theta\\\leq&e^{\beta t}\Big\{\dot{\mathcal{U}}(t)+(\beta+\eta_1 e^{\beta\bar{\varrho}}+\eta_2\bar{\imath}e^{\beta\bar{\imath}})\mathcal{U}(t)-\eta_1\mathcal{U}(\varrho(t))\hat{\varrho}-\eta_2\int_{t-\imath(t)}^{t}\mathcal{U}(v)\mathrm{d}v\Big\}\\=&e^{\beta t}\Big\{\dot{\mathcal{U}}(t)+\frac{\beta+\eta_1 e^{\beta\bar{\varrho}}+\eta_2\bar{\imath}e^{\beta\bar{\imath}}}{2}\int_{\underline{\alpha}}^{\overline{\alpha}}\hat{e}^T(t,\varsigma)\Lambda\hat{e}(t,\varsigma)\mathrm{d}\varsigma\\&-\frac{\eta_1\hat{\varrho}}{2}\int_{\underline{\alpha}}^{\overline{\alpha}}\hat{e}^T(\varrho(t),\varsigma)\Lambda\hat{e}(\varrho(t),\varsigma)\mathrm{d}\varsigma-\frac{\eta_2}{2}\int_{\underline{\alpha}}^{\overline{\alpha}}\int_{t-\imath(t)}^{t}\hat{e}^T(v,\varsigma)\Lambda\hat{e}(v,\varsigma)\mathrm{d}v\mathrm{d}\varsigma\Big\}.\end{aligned} \tag{18}$$

Thus, in view of the formulas (17) and (18),

$$\begin{aligned}\dot{\mathcal{W}}(t)\leq&e^{\beta t}\Bigg\{\int_{\underline{\alpha}}^{\overline{\alpha}}\hat{e}^T(t,\varsigma)\Big\{[\Lambda\mathcal{G}]^s-\Lambda\Big[\Big(\mathcal{A}-\sum_{r=1}^{3}\frac{\mathcal{B}_r\mathcal{B}_r^T}{2\varepsilon_r}-\big(\frac{\varepsilon_1 L_1+\beta+L_3 e^{\beta\bar{\imath}}\bar{\imath}^2}{2}\\&+\frac{\varepsilon_2 L_2 e^{\beta\bar{\varrho}}}{2\hat{\varrho}}\big)\mathbf{I}_n\Big)\otimes\mathbf{I}_{\mathcal{N}}\Big]\Big\}\hat{e}(t,\varsigma)\mathrm{d}\varsigma-\int_{\underline{\alpha}}^{\overline{\alpha}}\Big(\frac{\partial\hat{e}(t,\varsigma)}{\partial\varsigma}\Big)^T\Lambda(\mathcal{D}\otimes\mathbf{I}_{\mathcal{N}})\Big(\frac{\partial\hat{e}(t,\varsigma)}{\partial\varsigma}\Big)\mathrm{d}\varsigma\\&-\varpi^*\sum_{i=1}^{\mathcal{N}}\sum_{k=1}^{n}\int_{\underline{\alpha}}^{\overline{\alpha}}\xi_i^k e_i^k(t,\varsigma)e_i^k(t,\bar{\varsigma}_p)\mathrm{d}\varsigma\Bigg\}.\end{aligned} \tag{19}$$

In line with the analysis in the inequality (11), one has

$$\begin{aligned}&-\varpi^*\sum_{i=1}^{\mathcal{N}}\sum_{k=1}^{n}\int_{\underline{\alpha}}^{\overline{\alpha}}\xi_i^k e_i^k(t,\varsigma)e_i^k(t,\bar{\varsigma}_p)\mathrm{d}\varsigma\\\leq&-\varpi^*(1-\frac{\varepsilon_4}{2})\int_{\underline{\alpha}}^{\overline{\alpha}}\hat{e}^T(t,\varsigma)\Lambda\hat{e}(t,\varsigma)\mathrm{d}\varsigma+\frac{\delta^2\varpi^*}{2\varepsilon_4\pi^2}\int_{\underline{\alpha}}^{\overline{\alpha}}\Big(\frac{\partial\hat{e}(t,\varsigma)}{\partial\varsigma}\Big)^T\Lambda\frac{\partial\hat{e}(t,\varsigma)}{\partial\varsigma}.\end{aligned} \tag{20}$$

Substituting inequality (20) into inequality (19) yields that

$$\begin{aligned}\dot{\mathcal{W}}(t)\leq&e^{\beta t}\int_{\underline{\alpha}}^{\overline{\alpha}}\hat{e}^T(t,\varsigma)\Upsilon_1\hat{e}(t,\varsigma)\mathrm{d}\varsigma+e^{\beta t}\int_{\underline{\alpha}}^{\overline{\alpha}}\Big(\frac{\partial\hat{e}(t,\varsigma)}{\partial\varsigma}\Big)^T\Upsilon_2\Big(\frac{\partial\hat{e}(t,\varsigma)}{\partial\varsigma}\Big)\mathrm{d}\varsigma\\=&e^{\beta t}\int_{\underline{\alpha}}^{\overline{\alpha}}\tilde{\mathbf{E}}^T(t,\varsigma)\Theta\tilde{\mathbf{E}}(t,\varsigma)\mathrm{d}\varsigma,\end{aligned}$$

where $\tilde{\mathbf{E}}(t,\varsigma)=\Big(\hat{e}(t,\varsigma),\frac{\partial\hat{e}(t,\varsigma)}{\partial t}\Big)^T$, $\Upsilon_2=\Lambda\Big[\Big(\frac{\delta^2\varpi^*}{2\varepsilon_4\pi^2}\mathbf{I}_n-\mathcal{D}\Big)\otimes\mathbf{I}_{\mathcal{N}}\Big]$, $\Upsilon_1=[\Lambda\mathcal{G}]^s-\Lambda\Big[\Big(\mathcal{A}-\sum_{r=1}^{3}\frac{\mathcal{B}_r\mathcal{B}_r^T}{2\varepsilon_r}-\big[\frac{\varepsilon_1 L_1+\beta+\varepsilon_3 L_3 e^{\beta\bar{\imath}}\bar{\imath}^2}{2}+\frac{\varepsilon_2 L_2 e^{\beta\bar{\varrho}}}{2\hat{\varrho}}-(1-\frac{\varepsilon_4}{2})\varpi^*\big]\mathbf{I}_n\Big)\otimes\mathbf{I}_{\mathcal{N}}\Big]$ and

$$\Theta=\begin{pmatrix}\Upsilon_1 & 0\\0 & \Upsilon_2\end{pmatrix}.$$

By selecting $\varpi^*$, $\varepsilon_1$, $\varepsilon_2$, $\varepsilon_3$ and $\varepsilon_4$ appropriately such that $\Theta\leq 0$, one has $\dot{\mathcal{W}}(t)\leq 0$, which yields $\mathcal{W}(t)\leq\mathcal{W}(0)$.
On the other hand,

$$\mathcal{W}(t)\geq\mathcal{V}(t)\geq e^{\beta t}\frac{\lambda_{\min}(\Lambda)}{2}\|e(t,\cdot)\|^2_{[\underline{\alpha},\overline{\alpha}]}. \tag{21}$$

So,

$$\|e(t,\cdot)\|_{[\underline{\alpha},\overline{\alpha}]}\leq\kappa\sqrt{\mathcal{W}(0)}e^{-\frac{\beta}{2}t},\quad t\geq 0,$$

where $\kappa=\sqrt{\frac{2}{\lambda_{\min}(\Lambda)}}$. It implies that the RDNN (1) is asymptotically synchronized. □

**Remark 6.** In [40], Barbalat's lemma was used to prove the asymptotic synchronization of CNNs without diffusion terms under adaptive control. However, this analytical method cannot be directly applied to the synchronization analysis of RDNNs with mixed delays, because the existence of the diffusion term makes it impossible to guarantee the uniform continuity of $\mathcal{W}(t)$. Additionally,

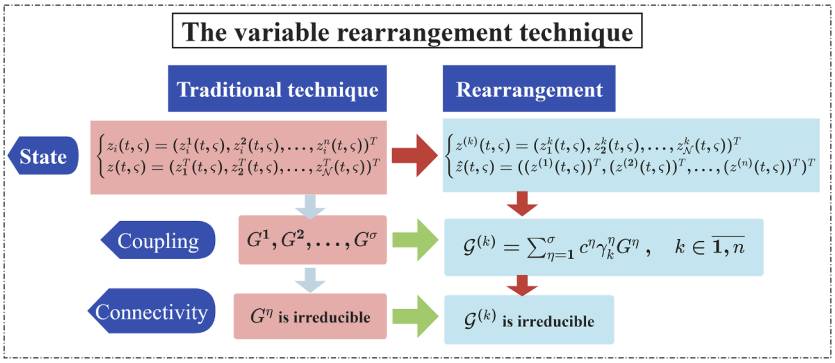


**Fig. 3.** Variable rearrangement technique.

in [16], based on reduction to absurdity, the asymptotic synchronization of RDNNs without delay was ensured under an adaptive strategy. Unfortunately, this method is also inapplicable to the RDNNs considered in this article due to the existence of mixed delays. Inspired by [29,31], an exponential term $e^{\beta t}$ was introduced into the construction of Lyapunov Krasovskii functionals and control design, the asymptotic synchronization of delayed RDNNs under adaptive control was successfully solved in Theorem 4. In fact, these methods can obtain the criteria of passivity and synchronization of RDNNs with mixed delays, but encountered the corresponding obstacles in research about the passivity-based synchronization. It is a topic that will be discussed in the future.

**Remark 7.** Based on the traditional variable arrangement, under the assumption that each coupling matrix is irreducible, several criteria based on each layer's coupling matrix were established to ensure the synchronization of multiweighted coupled neural networks [6–8]. However, in real-world scenarios, such assumptions may not always hold due to the complexity and variability of network structures. Furthermore, the calculation of the coupling matrices at each layer may increase the complexity of the synchronization condition verification. Interestingly, this assumption in this article is relaxed to the irreducibility of the weighted union matrices formed by all coupling layers through the variable rearrangement technique. As a result, several concise and easily verified passivity and synchronization criteria are derived in Theorems 1–4. The key techniques are presented in Fig. 3.

## 4. Numerical simulations

Two examples are provided to verify the passivity and synchronization results in this section.

**Example 1.** Consider a kind of RDNNs with mixed time-varying delays and 3-weighted couplings, whose dynamics satisfies Eq. (1), where $t \in \mathcal{R} \geq 0$, $\varsigma \in [-5,5]$, $\mathcal{D} = \mathcal{A} = 0.6\mathbf{I}3$, $c^1 = c^3 = 0.1$, $c^2 = 0.2$, $\Gamma^1 = \mathrm{diag}\{0.1,0.2,0.1\}$, $\Gamma^2 = \mathrm{diag}\{0.3,0.2,0.3\}$, $\Gamma^3 = \mathrm{diag}\{0.2,0.1,0.2\}$, the corresponding functions are given by Table 2, $\varsigma \in [-5+0.1p, -5+0.1(p+1)]$ ($p \in \overline{0,99}$) are the spatial sampling intervals, and the coefficient matrices

$$B_1 = \begin{bmatrix} 1 & 5 & 7 \\ -0.5 & 1 & 1.2 \\ 9 & 4 & -0.8 \end{bmatrix}, \quad B_2 = \begin{bmatrix} -0.1 & 3 & 5 \\ -2 & -0.2 & 1 \\ -2 & -5 & -0.1 \end{bmatrix}, \quad B_3 = \begin{bmatrix} 0.1 & -3 & -4 \\ 0.2 & 0.3 & -6 \\ 5 & 4 & 0.2 \end{bmatrix}.$$

The topology is given in Fig. 1, the weighted union communication topology is evidently strong connected with $\xi^{(1)} = \xi^{(2)} = \xi^{(3)} = 0.2\mathbf{1}_5$. By simple calculation, $L_1 = L_3 = 1$, $L_2 = 2$.

**Table 2**
Parameter selection.

| Delays and Nonlinear Activation Functions |
|---|
| $\varrho(t) = t - \frac{\exp(t)}{1+\exp(t)}$, with $\hat{\varrho} = 0.75$, |
| $\iota(t) = 0.5 + 0.2\sin(2\pi t)$, with $\bar{\iota} = 0.7$, |
| $f_1(z_i) = f_3(z_i) = (\tanh(z_i^1), \tanh(z_i^2), \tanh(z_i^3))^T$, |
| $f_2(z_i) = 2(\tanh(z_i^1), \tanh(z_i^2), \tanh(z_i^3))^T$. |
| The Initial and Boundary Conditions |
| $z(t,\varsigma)$ are given as arbitrary constants in $[-60,60]$, $(t,\varsigma) \in [-0.75,0] \times (-5,5)$, |
| $z_i(t,-5) = z_i(t,5) = \mathbf{0}_3$. |
| The Input and Output Vectors |
| $y_i(t,\varsigma) = Pe_i(t,\varsigma) + Q\bar{\omega}_i(t,\varsigma)$, $i \in \overline{1,5}$ with $P = 4\mathbf{I}_3$ and $Q = 5\mathbf{I}_3$. |
| $\omega_i(t,\varsigma) = \begin{pmatrix} 0.07i\sin(\frac{\pi}{2}+x)\cos(0.01t) \\ 0.09i\sin(\frac{\pi}{2}+x)\cos(0.005t) \\ 0.05i\sin(\frac{\pi}{2}+x)\cos(0.003t) \end{pmatrix}$. |

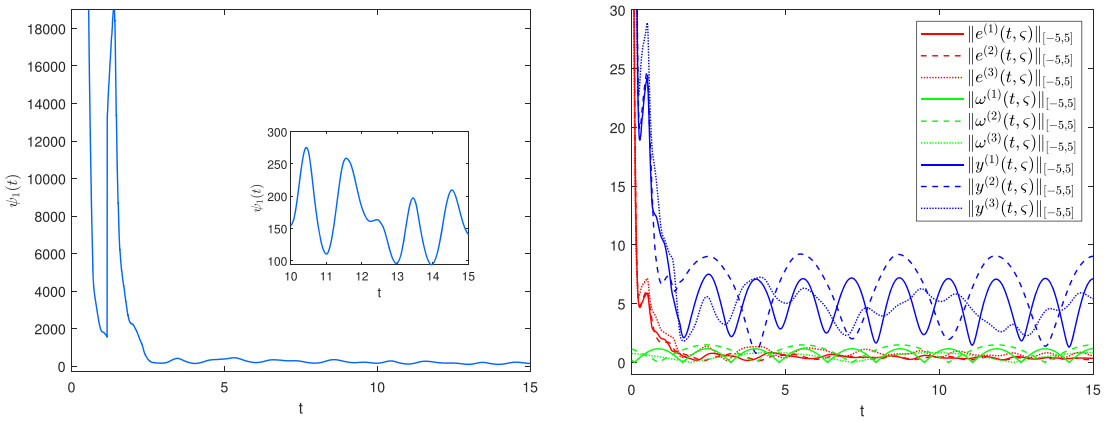


**Fig. 4.** Evolution of function $\psi_1(t)$ and the error $e_i^k(t,\varsigma)$ in Case I.

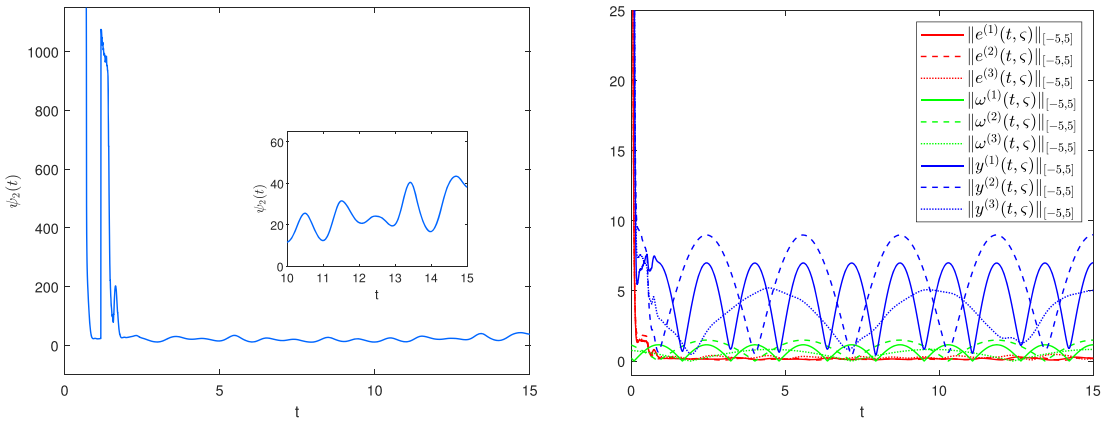


**Fig. 5.** Evolution of function $\psi_2(t)$ and the error $e_i^k(t,\varsigma)$ in Case II.

To verify the passivity of the error system (5), define

$$\psi_1(t) = \int_{\underline{\alpha}}^{\overline{\alpha}} \hat{y}^T(t,\varsigma)\mathcal{H}\hat{\omega}(t,\varsigma)\mathrm{d}\varsigma - \int_{\underline{\alpha}}^{\overline{\alpha}} \hat{\omega}^T(t,\varsigma)\mathcal{H}_1\hat{\omega}(t,\varsigma)\mathrm{d}\varsigma - \int_{\underline{\alpha}}^{\overline{\alpha}} \hat{y}^T(t,\varsigma)\mathcal{H}_2\hat{y}(t,\varsigma)\mathrm{d}\varsigma - \dot{V}(t),$$

$$\psi_2(t) = \int_{\underline{\alpha}}^{\overline{\alpha}} \hat{y}^T(t,\varsigma)\mathcal{H}\hat{\omega}(t,\varsigma)\mathrm{d}\varsigma - \int_{\underline{\alpha}}^{\overline{\alpha}} \hat{\omega}^T(t,\varsigma)\mathcal{H}_1\hat{\omega}(t,\varsigma)\mathrm{d}\varsigma - \dot{V}(t),$$

$$\psi_3(t) = \int_{\underline{\alpha}}^{\overline{\alpha}} \hat{y}^T(t,\varsigma)\mathcal{H}\hat{\omega}(t,\varsigma)\mathrm{d}\varsigma - \int_{\underline{\alpha}}^{\overline{\alpha}} \hat{y}^T(t,\varsigma)\mathcal{H}_2\hat{y}(t,\varsigma)\mathrm{d}\varsigma - \dot{V}(t).$$

**Case I.** To satisfy the conditions $C_1$ and $C_2$ in Theorem 1, choosing $\varepsilon_1 = \varepsilon_2 = \varepsilon_3 = 7$, $\varepsilon_4 = 2$, and by utilizing MATLAB LMI toolbox,

$$\mathcal{H} = \begin{bmatrix} 12.5585 & 0.1938 & -0.1117 \\ 0.1938 & 12.1270 & 0.0632 \\ -0.1117 & 0.0632 & 12.7263 \end{bmatrix} \otimes \mathbf{I}_5, \quad \mathcal{H}_1 = \begin{bmatrix} 17.6768 & 0.2102 & -0.1839 \\ 0.2353 & 17.1807 & 0.0642 \\ -0.0729 & 0.0813 & 17.8698 \end{bmatrix} \otimes \mathbf{I}_5,$$

$$\mathcal{H}_2 = \begin{bmatrix} 1.0974 & -19.8240 & 95.3621 \\ 19.8611 & 1.0562 & 10.5091 \\ 95.3833 & -10.4970 & 1.1134 \end{bmatrix} \otimes \mathbf{I}_5,$$

and the control gain $\varpi = 12.2429\mathbf{I}_5$. Under the spatial sampling controller (7), from Theorem 1, the strict passivity of error system (5) is achieved and shown in Fig. 4.

**Case II.** When $\mathcal{H}_2 = \mathbf{0}_{15}$, choose $\varepsilon_1 = \varepsilon_3 = 9$, $\varepsilon_2 = 6$, $\varepsilon_4 = 0.8$. By employing the MATLAB LMI toolbox, $\mathcal{H}, \mathcal{H}_1$ are solved as

$$\mathcal{H} = \begin{bmatrix} 0.1648 & -0.0692 & 0.0493 \\ -0.0692 & 0.3336 & -0.0254 \\ 0.0493 & -0.0254 & 0.1136 \end{bmatrix} \otimes \mathbf{I}_5, \quad \mathcal{H}_1 = \begin{bmatrix} 0.3278 & 31.5829 & 37.4941 \\ -31.8403 & 0.6412 & -20.3522 \\ -37.3136 & 20.2572 & 0.2337 \end{bmatrix} \otimes \mathbf{I}_5,$$

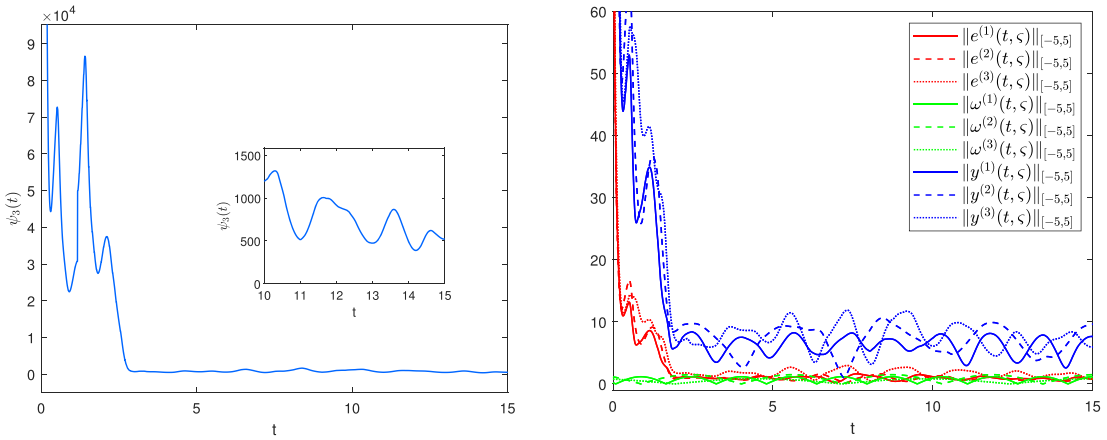


**Fig. 6.** Evolution of function $\psi_3(t)$ and the error $e_i^k(t,\varsigma)$ in Case III.

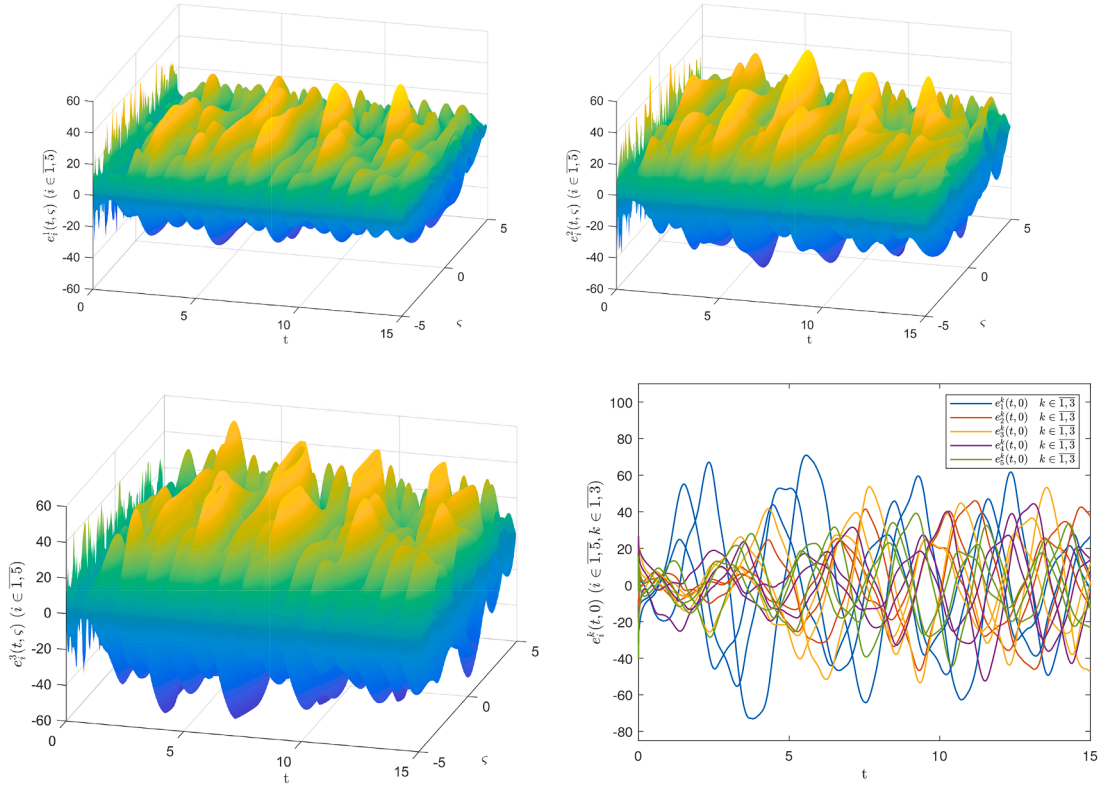


**Fig. 7.** Spatiotemporal evolution of $e_i^k(t,\varsigma)$ without control.

and control gain $\varpi = 36.1213\mathbf{I}_5$. Under the spatial sampling controller (7), the error system (5) is input-strictly passive and shown in Fig. 5.

**Case III.** When $\mathcal{H}_1 = \mathbf{0}_{15}$, select $\varepsilon_1 = 3$, $\varepsilon_2 = 6$, $\varepsilon_3 = 2$, and $\varepsilon_4 = 1.7$. By employing the MATLAB LMI toolbox, $\mathcal{H}$, $\mathcal{H}_2$ are calculated as

$$\mathcal{H} = \begin{bmatrix} 8.0862 & 0.9488 & -0.4061 \\ 0.9488 & 6.7500 & 0.2155 \\ -0.4061 & 0.2155 & 8.9455 \end{bmatrix} \otimes \mathbf{I}_5, \quad \mathcal{H}_2 = \begin{bmatrix} 0.7562 & 898.0732 & 455.6378 \\ -897.8896 & 0.6270 & -4.8870 \\ -455.7162 & 4.9288 & 0.8392 \end{bmatrix} \otimes \mathbf{I}_5.$$

and control gain $\varpi = 11.4197\mathbf{I}_5$. Based on Corollary 2, under the spatial sampling controller (7), the error system (5) is output-strictly passive and shown in Fig. 6.

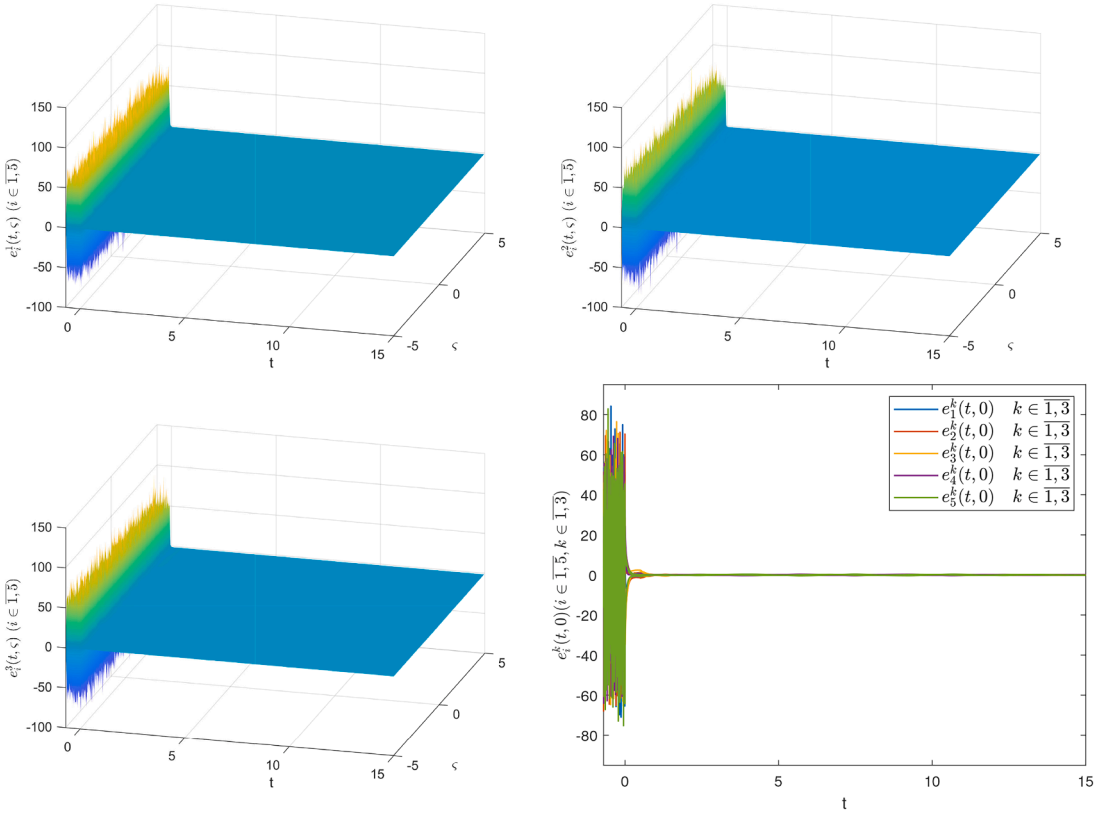


**Fig. 8.** Synchronization evolution under the spatial sampled-data controller (7).

Next, the asymptotic synchronization of the RDNN (1) is verified. Fig. 7 shows that the RDNN (1) fails to be synchronized in the absence of control. Under the spatial sampled-data controller (7), the error system (5) is output-strictly passive in Case III. When $\hat{\omega}(t,\varsigma)\equiv \mathbf{0}_{15}$, the network (1) is asymptotically synchronized, as ensured by Theorem 2 and illustrated by Fig. 8.

In what follows, the asymptotic synchronization of system (1) under adaptive spatial sampling controller (15) is verified. Choose $\beta=0.001$, $\delta_i=5$ and the initial conditions $\varpi_i(t,\varsigma)$ are given as the arbitrary constants in $[0,10]$ $(i\in\overline{1,5},\ (t,\varsigma)\in[-0.75,0]\times(-5,5))$. The asymptotic synchronization of the RDNN (1) with $\hat{\omega}(t,\varsigma)\equiv\mathbf{0}_{15}$ is achieved and shown in Fig. 9, and the dynamic of control gain $\varpi_i(t,\varsigma)$ is illustrated by Fig. 10.

**Example 2.** Based on the chaotic Logistic encryption scheme with the scrambling operation in [44], the passivity-based synchronization of RDNN (1) and the corresponding chaotic sequence are applied to image encryption and decryption via spatial sampling controller (7). The spatiotemporal chaotic behavior of $\bar{z}$ in the RDNN (1) is shown in Fig. 11.

The RDNN (1) and the weighted-average state (4) are regarded as receivers and sender, respectively. According to Example 1, the RDNN (1) is synchronized after $T0=5$. The flow of the encryption algorithm is shown in Fig. 12. The detailed steps are as follows.

**Step 1. Original image process.** Read the original image $I_0$ and resize it to $256\times256$. Separate color image $I_0$ into red, green, and blue components so that three pixel series are formulated, $A(h,j)$, $B(h,j)$, $C(h,j)$, $h\in\overline{1,256}$, $j\in\overline{1,256}$.

**Step 2. Chaotic signal process.** The chaotic sequences generated in system (4) are transformed to three security channels and denoted as $x,y,z$. Then, amplify the chaotic signals at a certain scale,

$$X=10000(x+5),Y=10000(y+5),Z=10000(z+5).$$

To facilitate the XOR operation, the scaled chaotic signals $X,Y,Z$ are converted into 8-bit integers $X_0,Y_0,Z_0$ by using the *im2uint8* function

$$X_0=\textit{im2uint8}(X),\ Y_0=\textit{im2uint8}(Y),\ Z_0=\textit{im2uint8}(Z).$$

Subsequently, rearranging the chaotic sequences $X,Y,Z$ to generate three new indexed sequences $l_x,l_y,l_z$. The color matrices $A,B,C$ of the original image are reshaped into three vectors $A_1,B_1,C_1$, i.e.,

$$A_1=\text{reshape}(A,1,n\mathcal{N}),\ B_1=\text{reshape}(B,1,n\mathcal{N}),\ C_1=\text{reshape}(C,1,n\mathcal{N}).$$

**Step 3. Encryption.** The encrypted pixel matrices of original image are generated by applying the following XOR operation

$$A_2=A_1\oplus X_0,\ B_2=B_1\oplus Y_0,\ C_2=C_1\oplus Z_0.$$

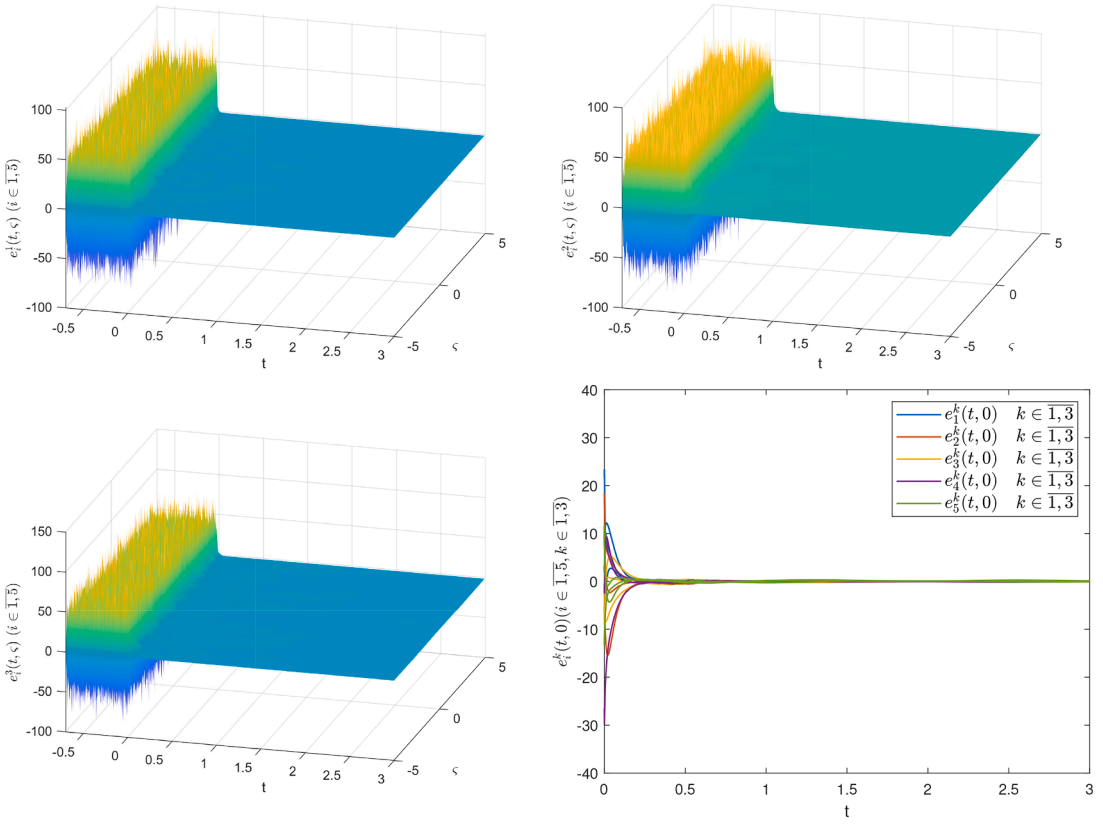


**Fig. 9.** Synchronization evolution under controller (15).

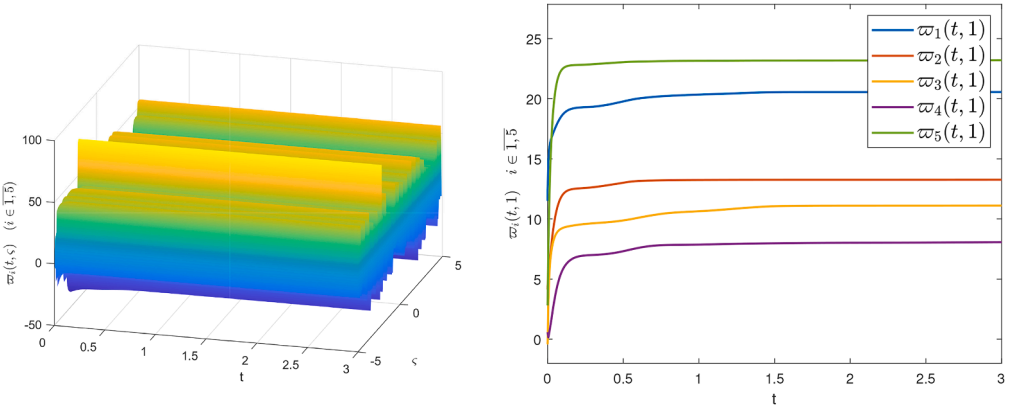


**Fig. 10.** Control gains $\varpi_i(t,\varsigma)$ in controller (15), $i\in\overline{1,5}$.

Then, rearranging the pixel values in $A_2, B_2, C_2$ based on indices $l_x, l_y, l_z$. Finally, the encrypted image $I_1$ is obtained by

$$A_3 = \text{reshape}(A_2, n, \mathcal{N}),\ \ B_3 = \text{reshape}(B_2, n, \mathcal{N}),\ \ C_3 = \text{reshape}(C_2, n, \mathcal{N}).$$

The decryption procedures are outlined as follows.

**Step 1. Original image process.** Read the original image $I_1$. Separate color image $I_1$ into red, green, and blue components so that three pixel series are yielded, $A_4(h,j)$, $B_4(h,j)$, $C_4(h,j)$, $h\in\overline{1,256}$, $j\in\overline{1,256}$.

**Step 2. Chaotic signal process.** The chaotic sequences generated in system (1) are transformed to three security channels and denoted as $x_1, y_1, z_1$. Then, amplify the chaotic signals at a certain scale,

$$X_1 = 10000(x_1+5),\ \ Y_1 = 10000(y_1+5),\ \ Z_1 = 10000(z_1+5).$$

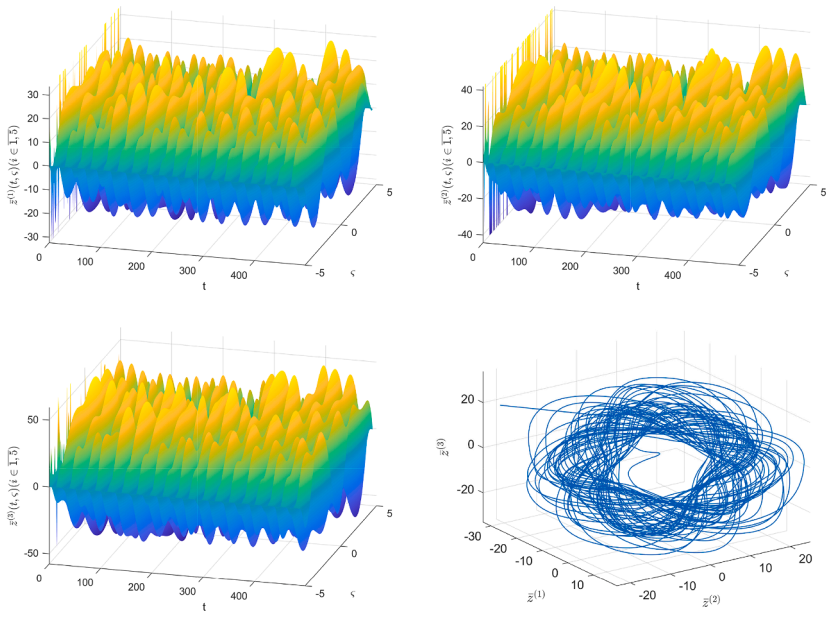

**Fig. 11.** The spatiotemporal chaotic behavior of the RDNN (1).

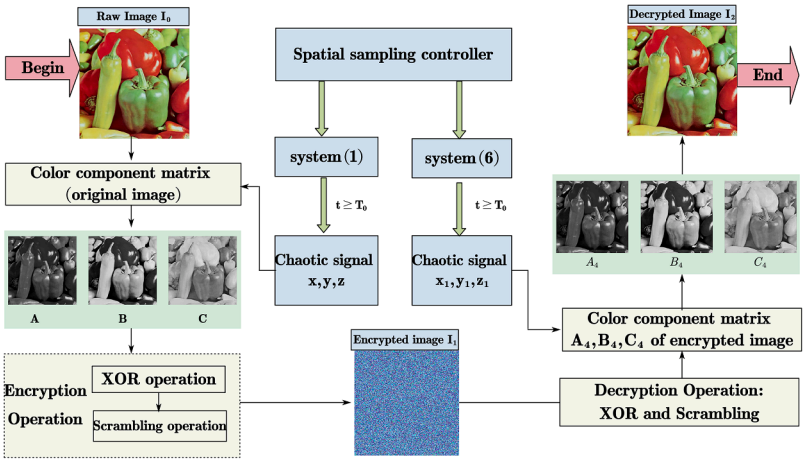


**Fig. 12.** Flow of image encryption and decryption.

To facilitate the XOR operation, the scaled chaotic signals $X_1$, $Y_1$, $Z_1$ are converted into 8-bit integers $X_0^{(1)}, Y_0^{(1)}, Z_0^{(1)}$ by using the *im2uint8* function

$$X_0^{(1)} = \textit{im2uint8}(X_1),\ Y_0^{(1)} = \textit{im2uint8}(Y_1),\ Z_0^{(1)} = \textit{im2uint8}(Z_1).$$

Subsequently, rearranging the chaotic sequences $X_1, Y_1, Z_1$ to generate three new indexed sequences $l_x^{(1)}, l_y^{(1)}, l_z^{(1)}$. The color matrices $A_4, B_4, C_4$ of the original image are reshaped into three vectors

$$A_5 = \text{reshape}(A_4, 1, n\mathcal{N}),\ B_5 = \text{reshape}(B_4, 1, n\mathcal{N}),\ C_5 = \text{reshape}(C_4, 1, n\mathcal{N}).$$

**Step 3. Decryption.** The encrypted pixel matrices of original image are generated by applying the following XOR operation

$$A_6 = A_5 \oplus X_0^{(1)},\ B_6 = B_5 \oplus Y_0^{(1)},\ C_6 = C_5 \oplus Z_0^{(1)}.$$

Then, rearrange the pixel values in $A_6, B_6, C_6$ utilizing indices $l_x^{(1)}$, $l_y^{(1)}$, $l_z^{(1)}$. Finally, the decrypted image $I_3$ is obtained by

$$A_7 = \text{reshape}(A_6, n, \mathcal{N}),\ B_7 = \text{reshape}(B_6, n, \mathcal{N}),\ C_7 = \text{reshape}(C_6, n, \mathcal{N}).$$

A 512 Ã– 512 grayscaling pepper image is selected as the test image shown in Fig. 13. The encrypted image is illustrated in Fig. 14, where the underlying image becomes indistinguishable. Through a series of reverse operations, the image is successfully decrypted, as

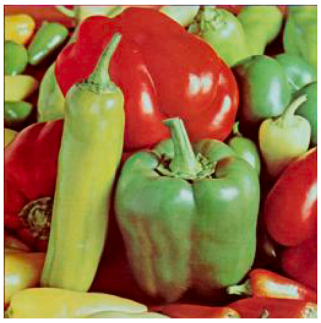

**Fig. 13.** Original Image.

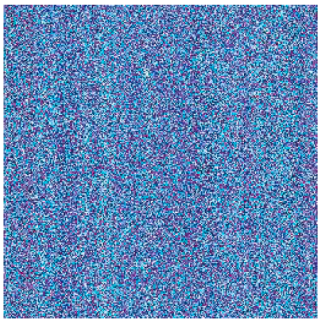

**Fig. 14.** Encrypted Image.

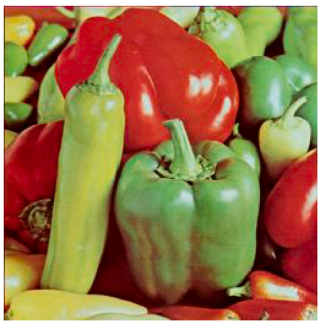

**Fig. 15.** Decrypted Image.

depicted in Fig. 15. Obviously, the decrypted image Fig. 15 is identical to the original image Fig. 13, which implies that the proposed passivity-based synchronization criteria and controller has reliable performance in image encryption and decryption.

## 5. Conclusion

This article investigated the passivity and synchronization of RDNNs with mixed delays and multi-weighted couplings based on spatial sampling control strategy. By constructing the Lyapunov Krasovskii functional, several passivity and synchronization criteria were derived by the technique of rearranging variable order and inequality skills. These conditions are determined by the diffusion coefficients, coupled strengths, time delays, sampling interval length and control parameters. An adaptive spatial sampling control scheme was proposed and the adaptive synchronization was rigorously analyzed. This control strategy integrates spatial sampling control with adaptive control, effectively reducing control costs and facilitating practical operation. Furthermore, the proposed passivity-based synchronization criteria and controllers have been applied to image encryption and decryption.

Recently, fixed-time/prescribed-time synchronization of complex networks were frequently considered in latest research [45], and the boundary limited-time synchronization of RDNNs has also emerged [46]. It inspires us to explore the limited-time passivity-based synchronization of RDNNs via spatial sampling control in the latest work.

## CRediT authorship contribution statement

**Haodong Cui:** Writing – original draft, Software, Methodology; **Haoyun Tang:** Writing – original draft, Software, Formal analysis; **Mingyu Ma:** Software, Methodology, Conceptualization; **Cheng Hu:** Writing – review & editing, Supervision, Funding acquisition; **Tingting Shi:** Validation, Supervision, Methodology.

## Data availability

No data was used for the research described in the article.

## Declaration of competing interest

The authors declare that they have no known competing financial interests or personal relationships that could have appeared to influence the work reported in this paper.

## Acknowledgments

This work was supported by National Research Innovation Program for undergraduates (202410755117), by Tianshan Talent Training Program (2022TSYCCX0013), by National Natural Science Foundation of China (Grant No. 62373317), by the Key Project of Natural Science Foundation of Xinjiang (2021D01D10), by the Basic Research Foundation for Universities of Xinjiang (XJEDU2023P023) and by Intelligent Control and Optimization Research Platform in Xinjiang University.

## References

[1] Liu HR, Liu MZ, Li DF, Zheng WF, Yin LR, Wang RL. Recent advances in pulse-coupled neural networks with applications in image processing. Electronics 2022;11(20):3264.
[2] Wu JB, Xu CL, Han X, Zhou DQ, Zhang ML, Li HZ, et al. Progressive tandem learning for pattern recognition with deep spiking neural networks. IEEE Trans Pattern Anal Mach Intell 2022;44(11):7824–40.
[3] Zhao Y, He X, Huang TW, Huang JJ. Smoothing inertial projection neural network for minimization $l_{p-q}$ in sparse signal reconstruction. Neural Netw 2018;99:31–41.
[4] Liu X. Synchronization and control for multiweighted and directed complex networks. IEEE Trans Neural Netw Learn Syst 2023;34(6):3226–33.
[5] Wang L, Didelot X, Yang J, Wong G, Shi Y, Liu WJ, et al. Inference of person-to-person transmission of covid-19 reveals hidden super-spreading events during the early outbreak phase. Nat Commun 2020;11(1):5006.
[6] Cao YT, Zhao LH, Zhong QS, Wen SP, Shi KB, Xiao JY, et al. Adaptive fixed-time output synchronization for complex dynamical networks with multi-weights. Neural Netw 2023;163:28–39.
[7] Aadhithiyan S, Raja R, Dianavinnarasi J, Alzabut J, Baleanu D. Robust synchronization of multi-weighted fractional order complex dynamical networks under nonlinear coupling via non-fragile control with leakage and constant delays. Chaos Solitons Fractals 2023;174:113788.
[8] Tong DB, MaB, Chen QY, Wei YB, Shi P. Finite-time synchronization and energy consumption prediction for multilayer fractional-order networks. IEEE Trans Circuits Syst II Express Briefs 2023;70(6):2176–80.
[9] Moylan P. Implications of passivity in a class of nonlinear systems. IEEE Trans Automat Contr 1974;19(4):373–81.
[10] Moeini N, Bahrami-Fard M, Shahabadini M, Azimi SM. Iman-eini h. passivity-based control of single-phase cascaded h-bridge grid-connected photovoltaic inverter. IEEE Trans Ind Electron 2023;70(2):1512–20.
[11] Willems JC. Dissipative dynamical systems. Eur J Control 2007;13(2):134–51.
[12] Wang JL, Zhao LH. Pd and pi control for passivity and synchronization of coupled neural networks with multi-weights. IEEE Trans Netw Sci Eng 2021;8(1):790–802.
[13] Hou MZ, Tan F, Duan GR. Finite-time passivity of dynamic systems. J Franklin Inst 2016;353(18):4870–84.
[14] Lin SR, Liu XW. Robust passivity and control for directed and multiweighted coupled dynamical networks. IEEE Trans Neural Netw Learn Syst 2023;34(12):10458–72.
[15] Zhang J, Zhu S. Passivity and robust passivity of impulsive inertial neural networks with proportional delays under the non-reduced order approach. Neurocomputing 2024;575:127322.
[16] Wang JL, Wu HN. Synchronization and adaptive control of an array of linearly coupled reaction-diffusion neural networks with hybrid coupling. IEEE Trans Cybern 2014;44(8):1350–61.
[17] Liu XZ, Wu KN, Zhang WH. Mean square finite-time boundary stabilisation and h∞ boundary control for stochastic reaction-diffusion systems. Int J Syst Sci 2019;50(7):1388–98.
[18] Wang ZY, Cao JD, Lu GP. Abdel-aty m. fixed-time passification analysis of interconnected memristive reaction-diffusion neural networks. IEEE Trans Netw Sci Eng 2020;7(3):1814–24.
[19] Wang JL, Wu HN, Huang TW, Ren SY, Wu JG. Passivity analysis of coupled reaction-diffusion neural networks with dirichlet boundary conditions. IEEE Trans Syst Man Cybern Syst 2017;47(8):2148–59.
[20] Wu KN, Zhou WJ, Liu XZ. Passivity-based boundary control for delay reaction-diffusion systems. J Franklin Inst 2022;359(9):4074–96.
[21] Huang YL, Lin SR, Yang EF. Event-triggered passivity of multi-weighted coupled delayed reaction-diffusion memristive neural networks with fixed and switching topologies. Commun Nonlinear Sci Numer Simul 2020;89:105292.
[22] Zhou L, Zhao Z. Delay-dependent passivity of impulsive coupled reaction-diffusion neural networks with multi-proportional delays. Commun Nonlinear Sci Numer Simul 2023;126:107415.
[23] Wang JL, Wu HN, Huang TW. Passivity-based synchronization of a class of complex dynamical networks with time-varying delay. Automatica 2015;56:105–12.
[24] Wang JL, Wu HN, Huang TW, Ren SY, Wu JG. Passivity and output synchronization of complex dynamical networks with fixed and adaptive coupling strength. IEEE Trans Neural Netw Learn Syst 2018;29(2):364–76.
[25] Sun Y, Hu C, Wen SP, Yu J, Jiang HJ. Pinning adaptive passivity and bipartite synchronization of leaderless fractional spatiotemporal networks. IEEE Trans Network Sci Eng 2025;12(1):319–31.
[26] Lin S, Huang Y, Ren S. Event-triggered passivity and synchronization of delayed multiple-weighted coupled reaction-diffusion neural networks with non-identical nodes. Neural Netw 2020;121:259–75.
[27] Wang YH. Event-triggered passivity and synchronization of multiple derivative coupled reaction-diffusion neural networks. Neurocomputing 2024;586:127619.
[28] Guan KZ, Yang JH. Global asymptotic stabilization of cellular neural networks with proportional delay via impulsive control. Neural Process Lett 2019;50:1969–92.

[29] Tu ZW, Ding N, Li LL, Feng YM, Zou LM, Zhang W. Adaptive synchronization of memristive neural networks with time-varying delays and reaction-diffusion term. Appl Math Comput 2017;311:118–28.
[30] Shi M, Tong DB, Chen QY, Zhou WN. Pth moment exponential synchronization for delayed multi-agent systems with léplxvy noise and markov switching. IEEE Trans Circuits Syst II Express Briefs 2024;71(2):697–701.
[31] Gu HB. Adaptive synchronization for competitive neural networks with different time scales and stochastic perturbation. Neurocomputing 2009;73(1):350–6.
[32] Ding K, Zhu QX, Huang TW. Prefixed-time local intermittent sampling synchronization of stochastic multicoupling delay reaction-diffusion dynamic networks. IEEE Trans Neural Netw Learn Syst 2024;35(1):718–32.
[33] Wu KN, Wang YZ, Wang Z. Spatial sampled-data control for stochastic reaction-diffusion systems. J Franklin Inst 2020;357(17):12538–54.
[34] Lu BL, Jiang HJ, Hu C, Abdurahman A, Liu M. H∞ output synchronization of directed coupled reaction-diffusion neural networks via event-triggered quantized control. J Franklin Inst 2021;358(8):4458–82.
[35] Wang ZP, Wu HN, Wang JL, Li HX. Quantized sampled-data synchronization of delayed reaction-diffusion neural networks under spatially point measurements. IEEE Trans Cybern 2021;51(12):5740–51.
[36] Wang ZP, Li QQ, Wu HN, Luo B, Huang T. Pinning spatiotemporal sampled-data synchronization of coupled reaction-diffusion neural networks under deception attacks. IEEE Trans Neural Netw Learn Syst 2023;34(10):7967–77.
[37] Zhao FL, Wang ZP, Qiao JF, Wu HN, Huang T. Adaptive event-triggered extended dissipative synchronization of delayed reaction-diffusion neural networks under deception attacks. Neural Netw 2023;166:366–78.
[38] Song X, Li X, Ahn CK, Song S. Space-dividing-based cluster synchronization of reaction-diffusion genetic regulatory networks via intermittent control. IEEE Trans Nanobiosci 2022;21(1):55–64.
[39] Song X, Wang M, Song S, Ahn CK. Intermittent state observer design for neural networks with reaction-diffusion terms using partial measurements. IEEE Trans Syst Man Cybern Syst 2023;53(8):5224–35.
[40] Li B. Pinning adaptive hybrid synchronization of two general complex dynamical networks with mixed coupling. Appl Math Model 2016;40(4):2983–98.
[41] Gu K, Chen J, Kharitonov VL. Stability of time-delay systems. New York, NY: Springer Science & Business Media; 2003.
[42] Liu K, Fridman E. Wirtinger'S inequality and Lyapunov-based sampled-data stabilization. Automatica 2012;48(1):102–8.
[43] Boyd S, Ghaoui LE, Feron E, Balakrishnan V. Linear matrix inequalities in system and control theory. Philadelphia, PA, USA: SIAM; 1994.
[44] Hui M, Liu XY, Zhu S, Cao J. Event-triggered impulsive cluster synchronization of coupled reaction-diffusion neural networks and its application to image encryption. Neural Netw 2024;170:46–54.
[45] Ma ZF, Tong DB, Chen QY, Zhou WN. Fixed/prescribed-time synchronization and energy consumption for kuramoto-oscillator networks. IEEE Trans Cybern 2025;55(7):3379–89.
[46] Shi TT, Hu C, Yu J, Zhu QX, Huang TW. Internal/boundary control-based fixed-time synchronization for spatiotemporal networks. IEEE Trans Cybern 2024;54(11):6693–706.